First Semi-Annual Progress Report,
for Period 2/1/90 - 7/31/90
for
NASA Marshall Space Flight Center
Grant No. NAG8-144

FRACTURE-TOUGH, CORROSION-RESISTANT BEARING STEELS

Northwestern University
Basic Industry Research Laboratory
1801 N. Maple
Evanston, Illinois 60201

Professor Gregory B. Olson, Principal Investigator

TABLE OF CONTENTS

LIST OF TABLES

LIST OF FIGURES

Summary

Research directed at the fundamental principles allowing design of stainless bearing steels with enhanced toughness and stress corrosion resistance has involved both investigation of basic phenomena in model alloys and evaluation of a prototype bearing steel based on a conceptual design exercise. Progress in model studies has included a scanning Auger microprobe (SAM) study of the kinetics of interfacial segregation of embrittling impurities which compete with the kinetics of alloy carbide precipitation in secondary hardening steels. These results can define minimum allowable carbide precipitation rates and/or maximum allowable free impurity contents in these ultrahigh strength steels. Characterization of the prototype bearing steel designed to combine precipitated austenite transformation toughening with secondary hardening shows good agreement between predicted and observed solution treatment response including the nature of the high temperature carbides. An approximate equilibrium constraint applied in the preliminary design calculations to maintain a high martensitic M_s temperature proved inadequate, and the solution treated alloy remained fully austenitic down to liquid nitrogen temperature rather than transforming above 200C. The alloy can be martensitically transformed by cryogenic deformation, and material so processed will be studied further to test predicted carbide and austenite precipitation behavior. A mechanistically-based martensitic kinetic model has been developed and parameters are being evaluated from available kinetic data to allow precise control of M_s temperatures of high alloy steels in future designs. Preliminary calculations incorporating the prototype stability results suggest that the transformation-toughened secondary-hardening martensitic-stainless design concept is still viable, but may require lowering Cr content to 9 wt. pct. and adding 0.5 to 1.0 wt. pct. Al. An alternative design approach based on strain-induced martensitic transformation during cryogenic forming, thus removing the high M_s constraint, may permit alloy compositions offering higher fracture toughness.

1.   Introduction

The Steel Research Group (SRG) is a multi-institutional basic research program directed at the scientific principles allowing design of a new class of ultrahigh strength (R_c55-60 hardness) steels with major improvements in fracture toughness and stress corrosion resistance. The research reported here is a part of that effort centered on design of an R_c60 martensitic stainless bearing steel for application in the SSME fuel and oxidizer turbopumps. Efforts in this first period have concerned both the investigation of fundamental phenomena and the characterization of a prototype bearing steel designed from tentative principles available thusfar.

Personnel involved during this period have included Prof. G.B. Olson, Principal Investigator, Dr. Gautam Ghosh, Research Associate (thermodynamic calculations and kinetic model development) and Research Technologist, Carol McCarus. Graduate students have included Research Assistant David Spaulding, working on interfacial embrittlement, and Graduate Fellow Charles Kuehmann, working on thermodynamic calculations and prototype characterization. Undergraduate student Anatol Bilyk, who headed the student project team designing the prototype bearing steel in the Materials Design class last Spring, participated in the prototype characterization as a Senior Thesis project. Research Assistant Professor Fu-Rong Chen and Graduate Fellow Jonathan Montgomery assisted in electron microscopy and microanalysis.

In the next period, the effort will be joined by Dr. Tom Kinkus, Research Associate (atom-probe microanalysis of carbide precipitation), Dr. Pete Jemian, Post-Doctoral Associate (Small-Angle Neutron Scattering study of carbide precipitation), and Research Scientist Dr. Semyon Vaynman (prototype characterization).

2.   Objectives and Approach

Initial objectives of the bearing steel design are to obtain an R_c60 hardness through-hardening martensitic stainless steel with twice the toughness and stress corrosion resistance of the 440C stainless currently used in the SSME turbopump application. This corresponds to a K_{Ic} of 40 MPa√m and a K_{ISCC} of 20 MPa√m. Visits were made this year to Pratt & Whitney-Florida on January 4 and to Rocketdyne/Rockwell on February 20 to present SRG research results and further discuss property objectives. While frictional heating during liquid oxygen cooling gives a steady state operating temperature near room temperature in the Rocketdyne bearing system, some degree

of lubrication achieved in the P&W system maintains an operating temperature closer to liquid oxygen temperature. Hence, cryogenic fracture toughness is an important concern. It was generally agreed that a reasonable objective would be to maintain a minimum toughness ratio of 50 pct. comparing liquid nitrogen temperature to room temperature. Potential objectives for future case/core systems were also discussed in terms of the Hertzian stress distribution during rolling contact. It appears plausible that a sufficiently tough R_c55 core could support a relatively thinner (~.010") R_c60 case achievable by ion-nitriding during secondary hardening at ~500C. Such case/core systems offer the greatest potential for fracture resistance, and will be explored in future work. Based on discussions with members of the Tribology Center at Northwestern, it is also anticipated that achieving R_c60 without coarse primary carbides, a feature of the "matrix steel' approach adopted here, will offer advantages in wear resistance compared to conventional R_c60 steels.

In contrast to the traditional methods of alloy development whereby a number of alloy compositions are simultaneously evaluated to provide empirical correlations between composition, processing and properties, the approach adopted here is based on a systems design philosophy in which mechanistic models are developed from theory and experiment in model systems, and prototype alloys are sequentially evaluated in an iterative process of design, evaluation, and reanalysis. The flow-block diagram in Figure 1 represents our view of an ultrahigh-strength martensitic steel as a system, identifying the important microstructural subsystems controlling the properties of interest, and the stages of processing affecting each. This diagram, and its relation to general principles of systems engineering which formed the basis of our Materials Design course, are discussed in a paper (1) attached here as an Appendix. The principles have also been highlighted in a previous short review paper (2).

3.   Basic Research

Progress of the overall SRG program in quantifying the important interrelations in Figure 1 have been thoroughly reviewed in an overview chaptér (3) of our recently published book (4). We will here highlight developments of particular importance to the bearing steel design. Figure 2 summarizes our comprehensive investigation (3) of M_2C carbide precipitation in AF1410 steel at 510C using a wide range of experimental techniques including atom-probe field-ion microanalysis (APFIM) and small-angle neutron scattering (SANS). Shown are the time dependence of (a) particle size, (b) particle shape (rod aspect ratio), (c) carbide composition, (d) carbide lattice parameters, (e) carbide composition, and (e) alloy hardness. The overall evolution is consistent with the nucleation and coarsening behavior predicted by theory of precipitation at high
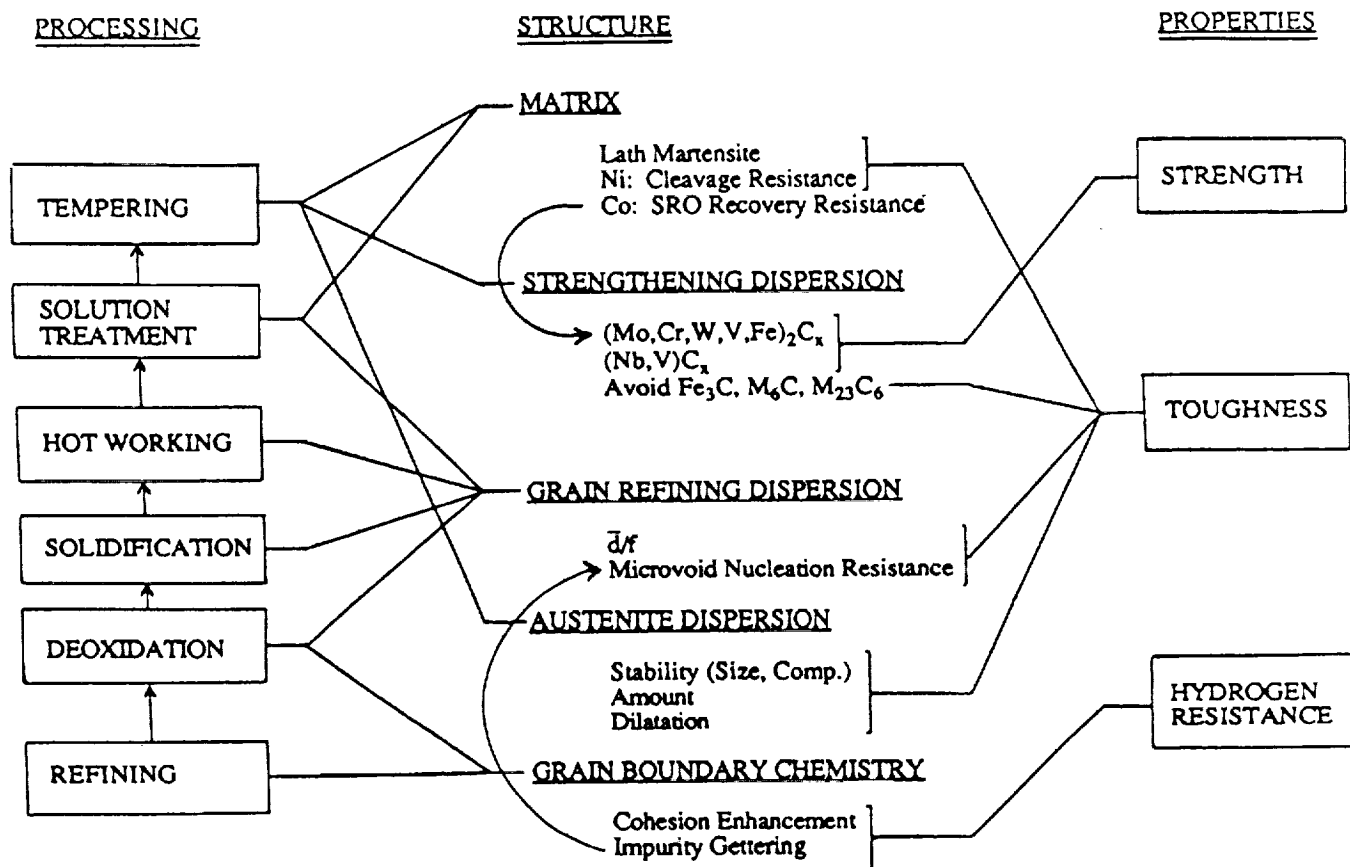
Fig. 1   Flow-block diagram illustrating the structure of Co-Ni secondary hardening steels as a system.
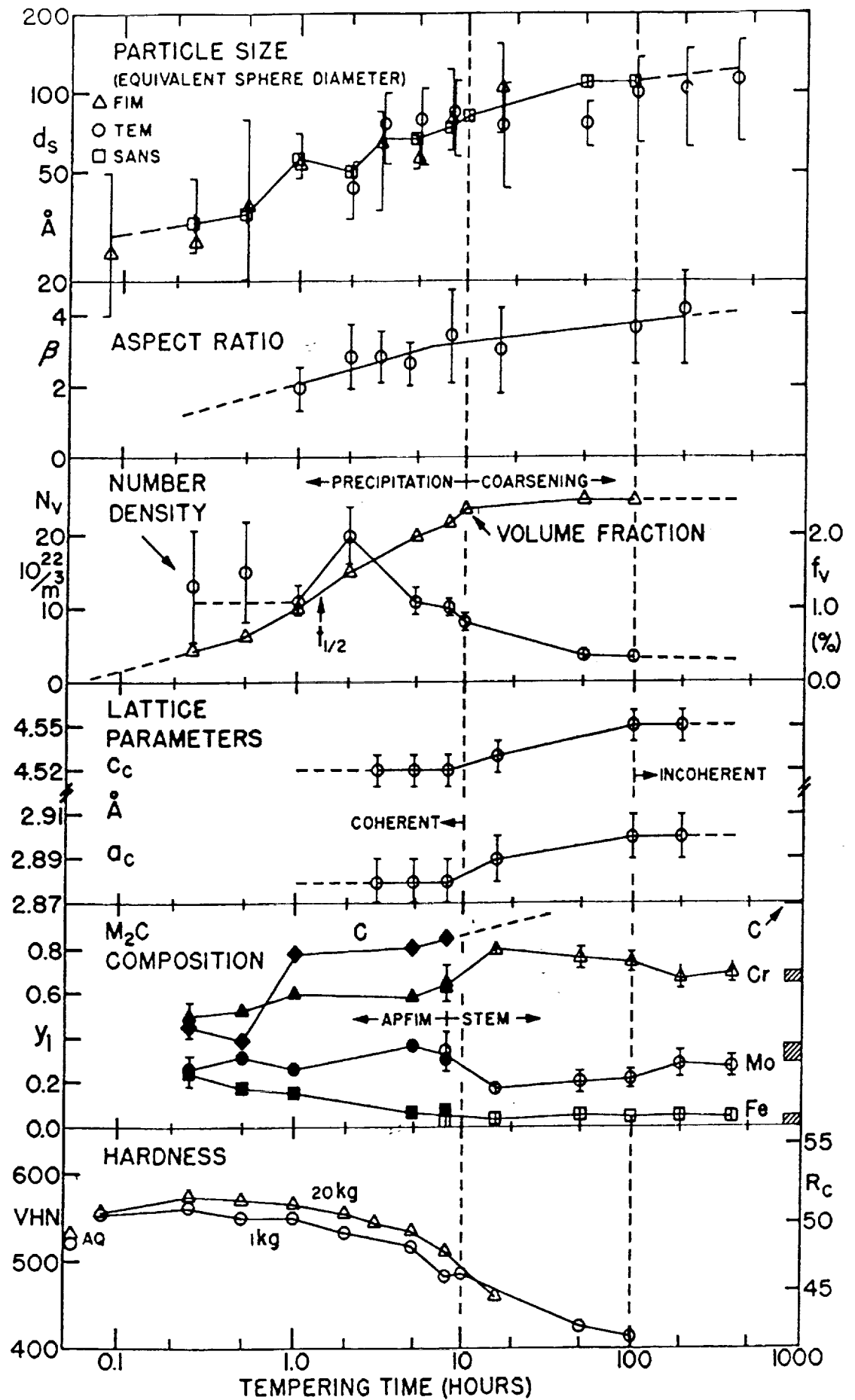
Fig. 2 M_2C carbide precipitation behavior in AF1410 steel vs. tempering time at 510C following 1 hr solution treatment at 830C.

4

supersaturations (5), but modified by strong departures of nucleus compositions from the final equilibrium values, attributable to a combination of elastic coherency and capillarity. A thorough analysis of elastic self energy and dislocation interaction energy (6) has been incorporated in a treatment of heterogeneous coherent nucleation on dislocations fit to measured nucleation rates and critical nucleus sizes (7). The observed carbide composition trajectory appears consistent with initial nuclei adopting compositions of low interfacial energy and then following a trajectory of increasing interfacial energy compensated by an increasing precipitation driving force which maintains continued nucleation. This newly observed phenomenon is important to the high overaging resistance shown by the hardness curve of Figure 2. The overaging resistance is essential to these alloys since, as indicated in Figure 1, it is necessary to bring the M_2C carbide precipitation to completion in order to eliminate the metastable Fe_3C which forms earlier and limits fracture toughness (8).

Precipitation phenomena are also being investigated in the series of model alloys compared with AF1410 in Table 1. These provide a test of model predictions of the two important scaling factors controlling precipitation behavior: (a) the coarsening rate constant and (b) the initial critical nucleus size. Coarsening rates have been measured and show reasonable agreement with model prediction (3,9,10). Critical nucleus size will be tested in future SANS studies. The latter is the most important factor in controlling strength, and scales inversely with the coherent precipitation driving force. Composition design for efficient strengthening without embrittlement has been approached applying our thermodynamic models to maximize the coherent M_2C driving force (for particle size refinement) while maintaining limits on the driving force for competing embrittling carbides such as M_6C (11). Contour plots illustrating this approach are shown in Figure 4 of the Appendix. While the experimental studies of AF1410 and the model alloys have so far been conducted under other sponsorship (primarily NSF and AFOSR), the continued APFIM and SANS studies necessary to further model refinement will be performed under the subject NASA grant in the next period.

Studies (12,13) conducted under NSF and ARO support have predicted enhanced toughness with refinement of particle size of grain refining dispersions (Figure 1) achievable with rapid solidification processing (3), and experiments indicate Ti compounds such as TiC show superior interfacial cohesion for toughening through microvoid nucleation resistance (3,13). Procedures have also been demonstrated for optimization of solution treatments to enhance toughness through modification of grain refining dispersions (14). As also denoted in Figure 1, further toughening can be achieved from metastable precipitated austenite dispersions of optimal thermodynamic stability for transformation toughening. Under DOE sponsorship, studies of

Table 1
Alloy Steel Compositions (wt. pct.)

Commercial	C	Co	Ni	Mo	Cr
AF1410	0.16	14.25	10.15	1.05	2.10
Experimental					
1) 1410-4Mo	0.23	14.17	10.24	3.96	0.06
2) 1605-4Mo	0.24	15.99	4.96	4.03	0.02
3) 1605-MoCr	0.24	16.08	4.79	2.82	0.71
4) 1605-CrMo	0.24	16.06	4.98	1.52	1.40

transformation toughening in model austenitic steels have achieved a K_{IC} of 340 MPa$\sqrt{m}$ at a yield strength of 1350 MPa and clarified the optimum stability for toughening (15). Our previous experiments have demonstrated the corresponding toughening effect of precipitated austenite dispersion in AF1410 steel (16) and a model is being developed under ARO support to predict austenite compositions with enhanced transformation dilatancy for further transformation toughening (17).

The fundamental mechanism by which grain boundary chemistry (Figure 1) controls intergranular hydrogen stress corrosion resistance in these steels is being investigated under ONR sponsorship with supercomputer support from NSF. Theory of the thermodynamics and mechanics of embrittlement (18) has predicted that the embrittling potency of intergranular segregants (including hydrogen) scales with the difference in segregation energies at grain boundaries and free surfaces, supported by available surface thermodynamic data. The electronic basis of these thermodynamic quantities controlling embrittlement has now been examined by all-electron total-energy calculations providing detailed comparison of electronic structure and bonding of phosphorus atoms in grain boundary and corresponding fracture surface environments, and comparisons of the states of B,C,P, and S in the grain boundary environment (3,19). Electronic features correlating with embrittlement will ultimately allow design of grain boundary composition for enhanced intrinsic cohesion and resistance to hydrogen interaction.

Dramatic improvements in K_{ISCC} in an R_c57 model NiMo steel have been demonstrated by removing P from grain boundaries via gettering by lanthanum phosphate which can be produced by high melt undercooling during rapid solidification (20). Our first attempt to reproduce the results in a larger heat failed due to lanthanum silicate formation attributed to crucible contamination. Processing optimization is being investigated further (21) by the Army Materials Technology Laboratory (MTL). Six heats with variations in melt deoxidation practice have been prepared and are undergoing evaluation. It is planned that the optimum processing condition thus identified will ultimately be applied to the bearing steels of concern here once a suitable alloy composition is demonstrated.

Under the subject NASA grant, intergranular temper embrittlement encountered in the model alloys of Table 1 has been investigated by scanning Auger microanalysis (SAM). After earlier preliminary Auger measurements had failed to indicate intergranular impurity segregation associated with the observed smooth intergranular fracture, some preliminary electron microscopy gave evidence of embrittlement by intergranular M_6C carbide precipitation. However, further electron microscopy has not provided convincing support for M_6C precipitation, and so a more

thorough Auger study has been undertaken by graduate student David Spaulding. To enhance the intergranular fracture behavior, specimens were hydrogen charged prior to room temperature impact fracture in the Auger spectrometer. As shown by the Auger spectrum of Figure 3, alloy 2 aged 5 hrs at 510C shows significant P and S segregation. A greater amount is also detected after 100 hrs tempering. Further studies will examine the segregation kinetics as a function of temperature. It thus appears that in alloys of commercial purity, carbide precipitation strengthening must kinetically compete with impurity segregation such that optimum properties will require acceleration of M_2C precipitation to reach completion before significant segregation. Alternatively, the same gettering techniques being examined for improved hydrogen stress-corrosion resistance may allow use of more slowly precipitating compositions once segregating impurities are effectively eliminated.

4. Design

As described in detail in our original proposal and summarized in the Appendix, a team of students in the Materials Design class at Northwestern employed the tentative principles available from this research in the Spring of 1989 to undertake the conceptual design of a transformation toughened martensitic stainless bearing steel. Briefly, the composition was constrained for compatability with rapid solidification and lanthanum treatment for stress corrosion resistance. Based on the strengthening data from the model alloys of Table 1, a carbon content of 0.30 wt. pct. was estimated to achieve R_c60 hardness. The matrix was constrained to contain 12 Cr for general corrosion resistance. A line of compositions in Ni and Co was then calculated (Appendix Figure 5) to maintain a sufficiently high martensitic T_o (partitionless equilibrium) temperature to obtain a lath martensite microstructure. It should be noted here that it was recognized that directly constraining the M_s martensite start temperature would be more desirable, but insufficient martensite kinetic parameters were available at that time. Unique Ni and Co contents were then defined by the amount and thermodynamic stability of the austenite that could be precipitated during secondary hardening near 500C. Mo and V contents were then optimized for relative precipitation driving forces (as in Appendix Figure 4). The V level was ultimately set by solution treatment conditions (Appendix Figure 6). This then defined a unique 7 component composition of Fe-30Co-12Cr-6Ni-0.3Mo-0.25V-0.30C. To ensure internal consistency in the sequence of calculations and to permit higher alloy Ni content for cleavage resistance, a second iteration calculation was performed by C. Kuehmann yielding the related composition Fe-22.6Co-12Cr-8.6Ni-0.3Mo-0.25V-0.30C. A small heat of this composition was then requested from Carpenter Steel for evaluation.
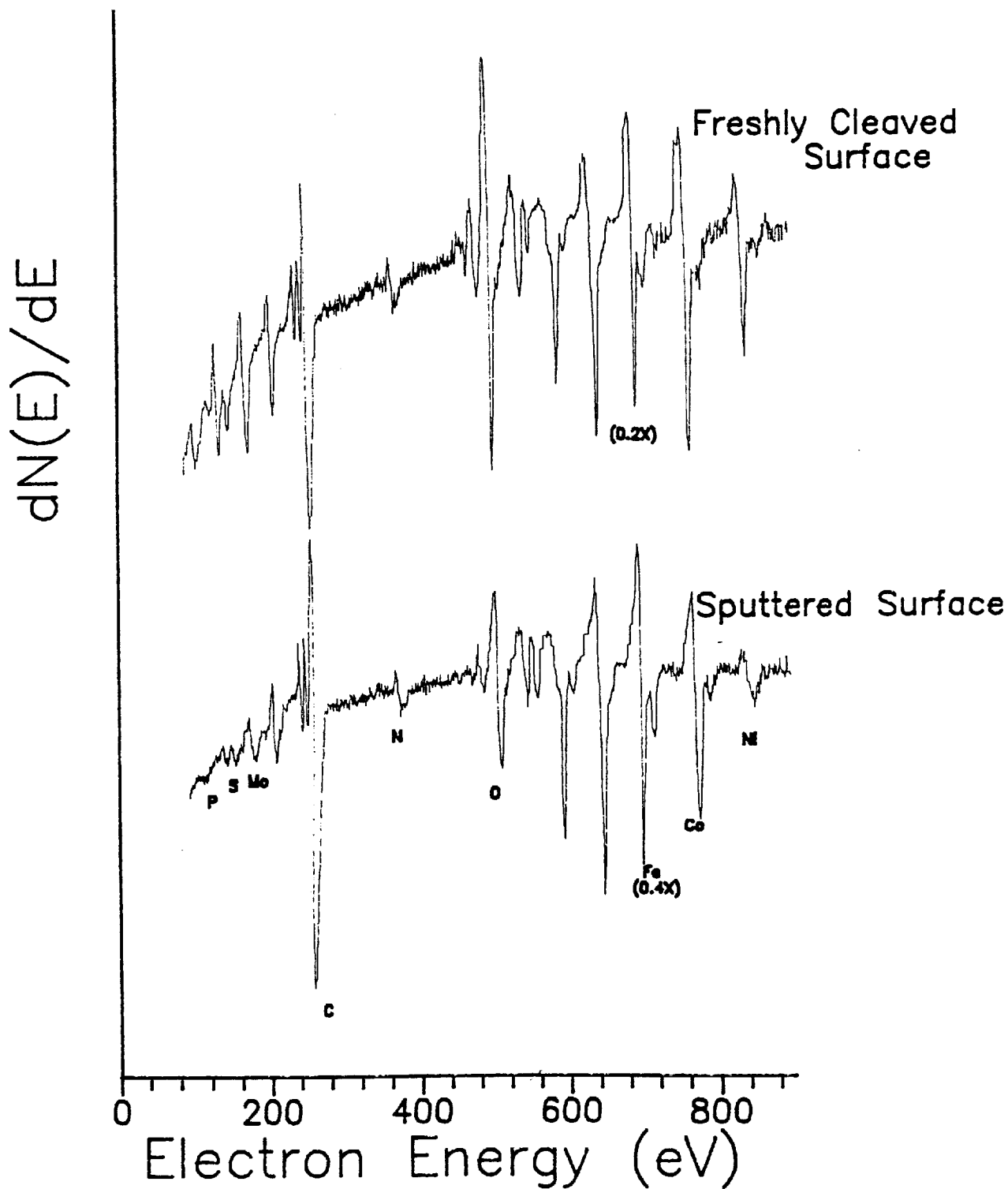
8

Fig. 3   Auger electron spectrum from SAM analysis of intergranular fracture facet from
hydrogen charged 16Co-5Ni-4Mo-0.25C steel tempered 5 hr at 510C (1000C
solution treat). Reduced relative heights of P and S peaks with sputtering
demonstrate intergranular segregation.

5. Prototype Characterization

A 17 pound vacuum induction heat of the requested composition was melted at Carpenter Steel and treated with 2g of Cerium prior to casting in a 2.75" sq. tapered ingot mold. The composition obtained is given in Table 2. The ingot was held 1 hr at 2100°F and forged to .75" sq. pilot bar and air cooled.

The as-received air cooled material showed a hardness of ~R_c45 with a retained austenite content of 30 pct., apparently transformed primarily to bainite during the air cool. Macroetching of the sectioned bar (Picral etch) showed the inhomogeneous deformation pattern from forging shown in Figure 4. Shear localization during hot work resulted in an "X" pattern of highly worked fine grained material surrounded by lightly worked "dead zones" of material showing the original ingot microsegregation patterns. Specimens for microstructure and property evaluation were selectively removed from the fine grained material.

Xray microprobe analysis indicated a reasonably uniform composition, as summarized in Table 3 for the differently etching areas of Figure 4. Microhardness indicated surface decarburization to a depth of 0.35mm.

Figure 5 summarizes the thermodynamic prediction (from ThermoCalc) of the equilibrium phase distribution vs. temperature for this alloy composition. Ferrite is fully transformed to austenite above 760C, and two equilibrium carbides exist, $(Cr,Mo)_{23}C_6$ and Cr_7C_3 which are fully dissolved above 1065C. Based on these predictions solution treatment response was investigated in a series of specimens electric-discharge machined from the fine-grained material and treated 1 hr at temperatures ranging from 1025 to 1150C. For investigation of austenite grain structure, a metallographic etch was developed for this material consisting of 50ml HCl, 10ml HF, with 15ml 3% H_2O_2. Austenite grain size and resulting microhardness after water quenching quartz encapsulated specimens from the solution treatment temperature are summarized in Figure 6. Below 1100C a pronounced duplex grain structure is associated with incomplete carbide dissolution. The overall average grain size is plotted in Figure 6 along with approximate average values of the large and small grain populations Uniform grain size and a constant hardness level were achieved at 1100C and above suggesting full solution treatment in line with equilibrium predictions. Electron microscopy of carbon extraction replicas from material treated at 1100, 1125, and 1150C shown in Figure 7 indicate that 1 hr treatment is insufficient to reach full equilibrium.

10

Table 2 - Composition of V00743 Melted for Northwestern University

C	0.29
Mn	<.01
Si	.01
P	.005
S	.003
Cr	11.75
Ni	8.48
Mo	0.30
V	0.25
Co	22.53
Ce	<.001
La	<.001

1.0 cm
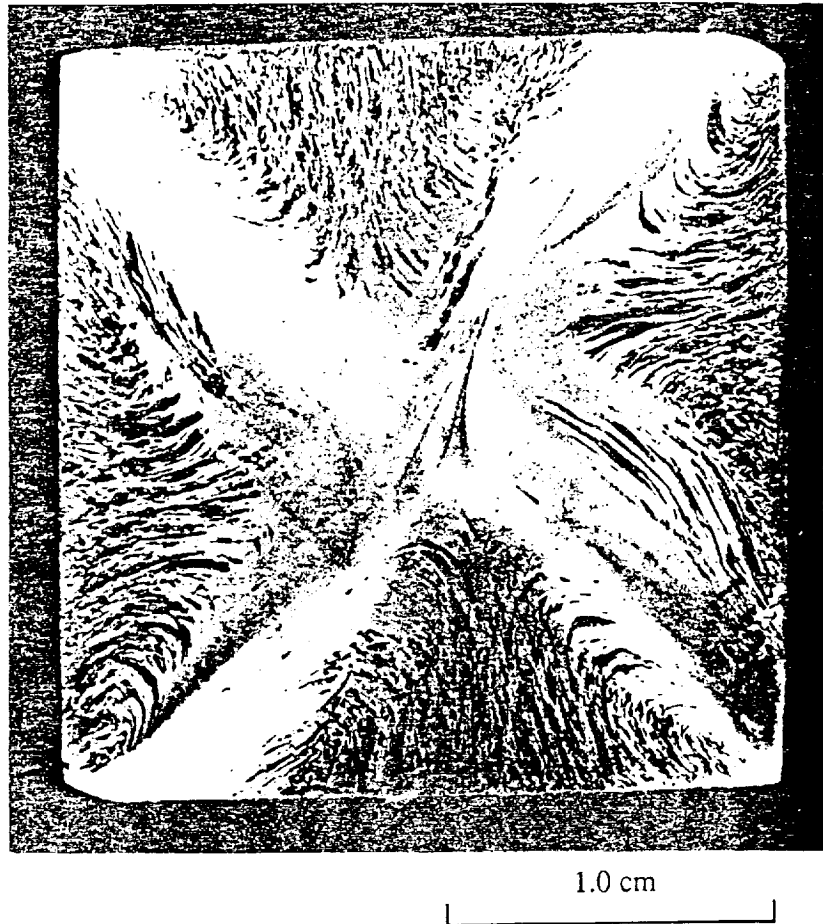
Fig. 4   Macro-etched section of as-forged bar of prototype bearing steel.

Table 3 SEM Energy Dispersive X-ray
Microanalysis of Forged Bar (wt. pct.)

Area	Fe	Cr	Co	Ni	V	Mo
Fine Grained	55.79	11.87	23.57	8.54	0.23	0.00
Coarse Grained-dark etching	56.53	11.17	23.79	8.12	0.24	0.15
Coarse Grained-bright etching	55.74	11.48	23.44	8.73	0.38	0.22
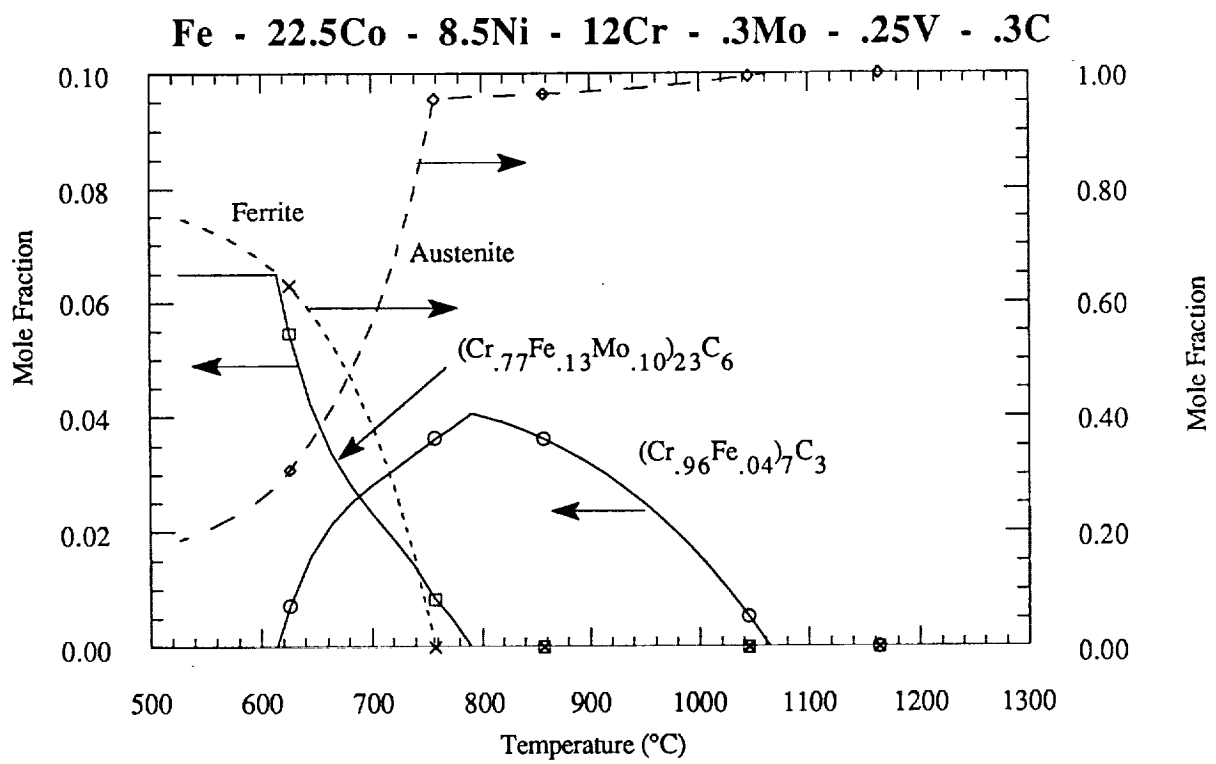
Fig. 5   Thermo-Calc computed phase distribution vs. temperature for prototype bearing steel.

Fe-22.5Co-8.5Ni-12Cr-.3Mo-.25V-.3C
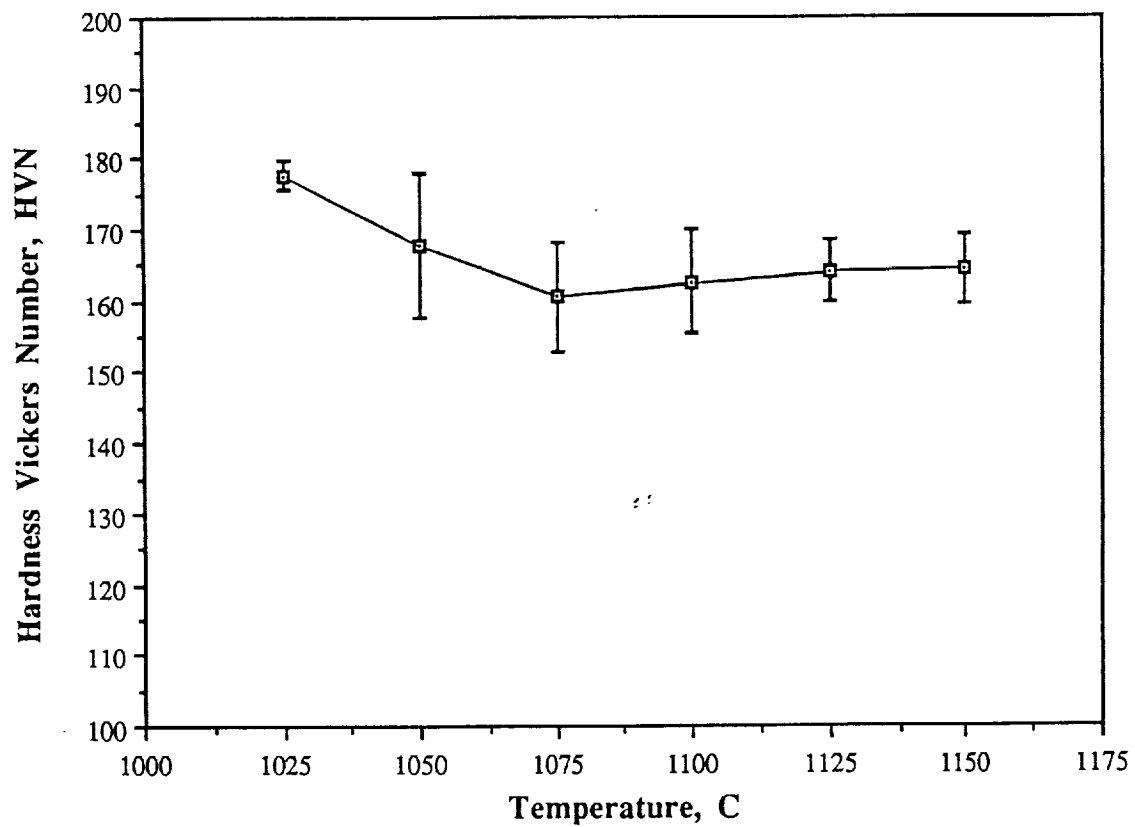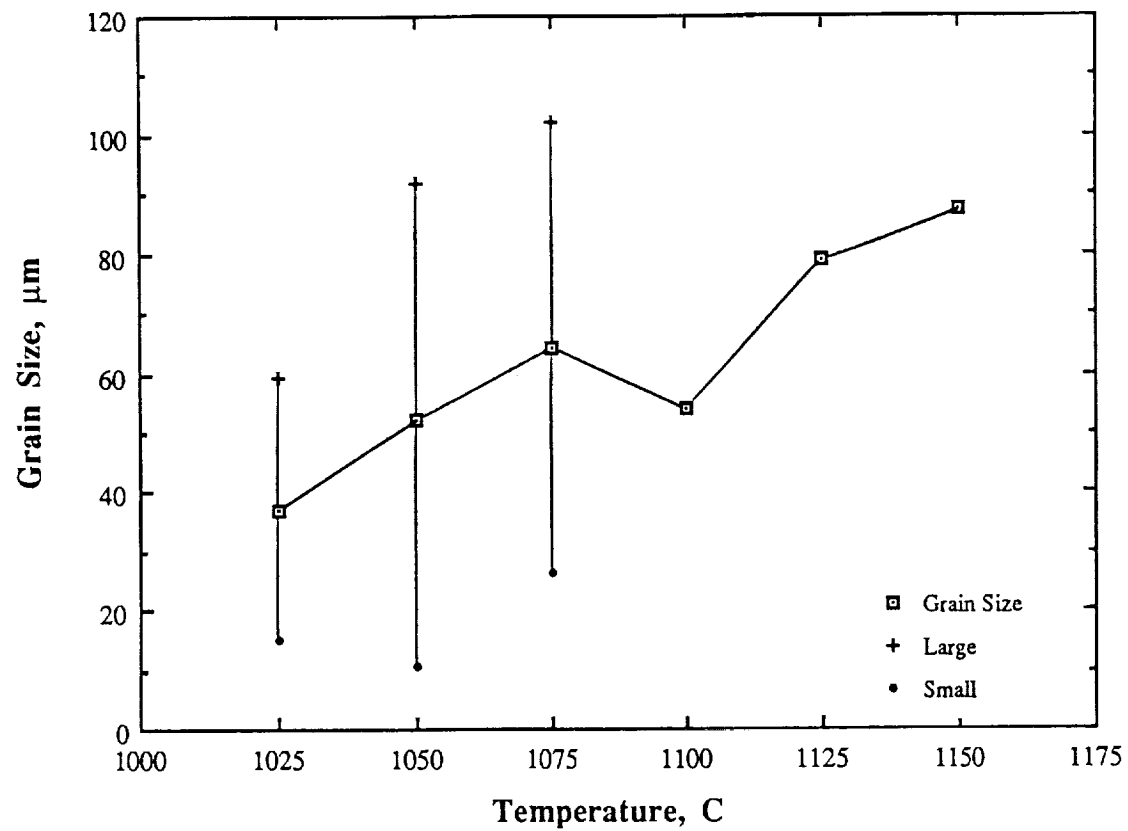
Fig. 6   Austenite grain size and as-quenched hardness vs. solution temperature for prototype bearing steel.

A significant amount of fairly coarse 1 μm scale carbides are still present at 1100C, dissolving at higher temperatures to leave finer ~0.2μm scale residual carbides controlling the austenite grain size. Xray microanalysis of these carbides in the scanning transmission electron microscope (STEM) indicated the presence of two types of carbides at all of these temperatures. The STEM Xray spectra shown in Figure 8 confirm the two types consist of a Cr-Mo carbide and a Cr carbide. This is in line with equilibrium prediction except that the distribution of the two types with temperature does not follow the equilibrium prediction, suggesting nonequilibrium conditions at 1 hr treatment times. Vanadium is found to be present in these two carbides rather than a separate carbide, consistent with prediction. Overall, solution treatment response compares reasonably well with equilibrium predictions. The relatively coarse grain sizes associated with solution treatment at 1125-1150C indicate the need for an independent coarsening resistant grain refining dispersion, as can be achieved through rapid solidification processing.

While solution treatment response showed reasonable agreement between theory and experiment, a major discrepancy was encountered in the primary FCC→BCC martensitic transformation behavior. Although the air cooled forgings, in which significant carbon was tied up in carbides, achieved a predominately BCC structure through bainitic transformation on cooling, fully solution treated material remained fully austenitic not only on quenching to room temperature, but even on cooling to liquid nitrogen temperature. In hindsight this underestimate of the austenite stability can be attributed to a combination of the inadequacy of the tentative equilibrium T_o constraint relative to the desired M_s kinetic constraint, and the drive to increase Ni content (an austenite stabilizer) for cleavage resistance. The result places a high priority on development of an adequate martensite kinetic model to control M_s temperatures in these complex high alloy compositions.

Based on the transformation behavior of the air cooled forging, a dilatometric study was undertaken to investigate possible bainitic transformation of this alloy. Although a detectable dilation outlined the C-curve depicted in Figure 9 with a nose temperature near 420C characteristic of a bainitic reaction, calibration with Xray diffraction showed a negligible amount of bainitic transformation could be achieved in this alloy.

Achieving a BCC structure through strain-induced martensitic transformation was next investigated performing tensile tests of 1150C solution treated material. After fabrication of suitable low temperature testing fixtures, tests were conducted at -60C in methanol and -196C in liquid nitrogen. While the -60C test showed a conventional downward curving σ–ε curve, the -196C curve of Figure 10 showed the sigmoidal shape and high strain hardening characteristic of
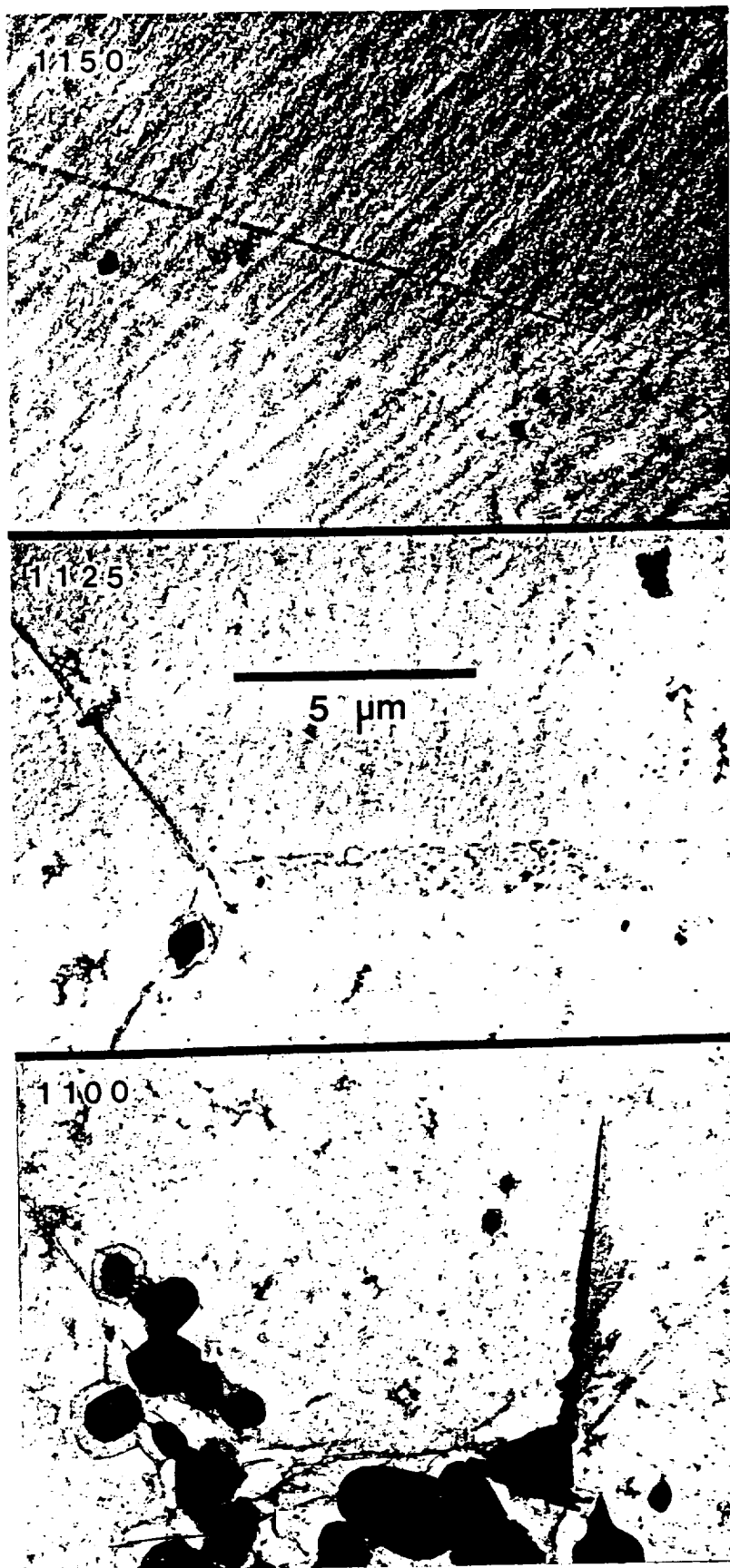
Fig. 7   Transmission electron micrographs of carbon extraction replicas showing carbides remaining after solution treatment of prototype bearing steel at 1100-1150C.

MoLα   CrKα   CuKα

V Kα

2.00   4.00   6.00   8.00

O C N T   O . O O K E V   1OeV/ch A   E D A X

CrKα

CuKα

FeKα

CoKα

V Kα

2.00   4.00   6.00   8.00

O C N T   O . O O K E V   1OeV/ch A   E D A X
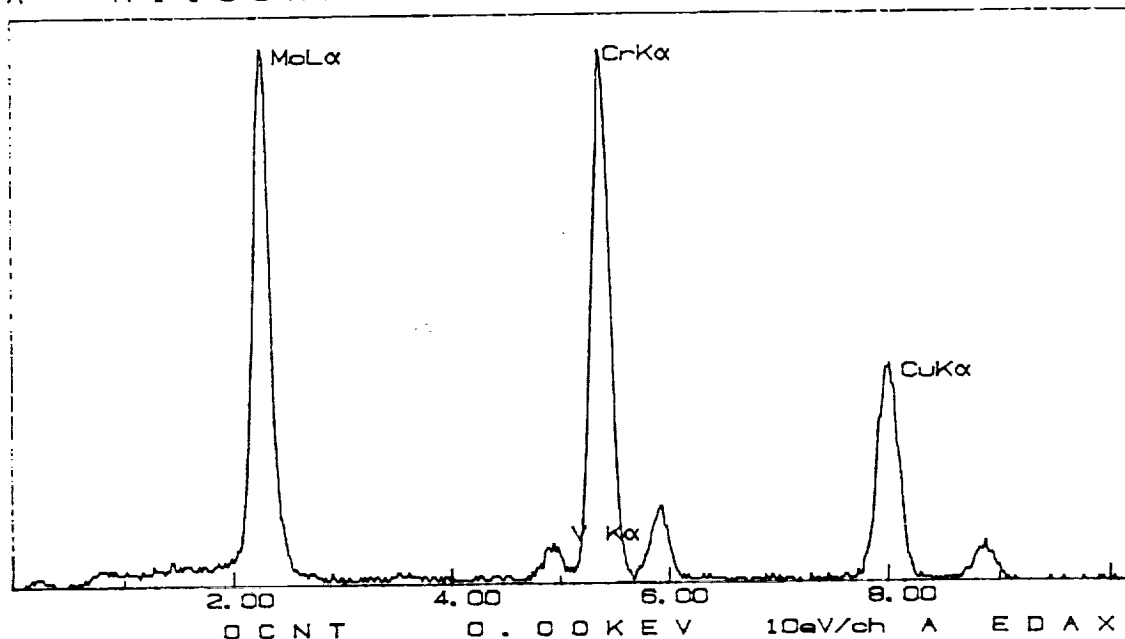
Fig.8   X-ray fluorescence spectra obtained from STEM microanalysis of two types of carbides present in structures of Fig. 7, showing both Cr-Mo and Cr-rich carbides.

18

TTT Curve

Fe - 22.5Co - 8.5Ni - 12Cr - .3Mo - .25V - .3C
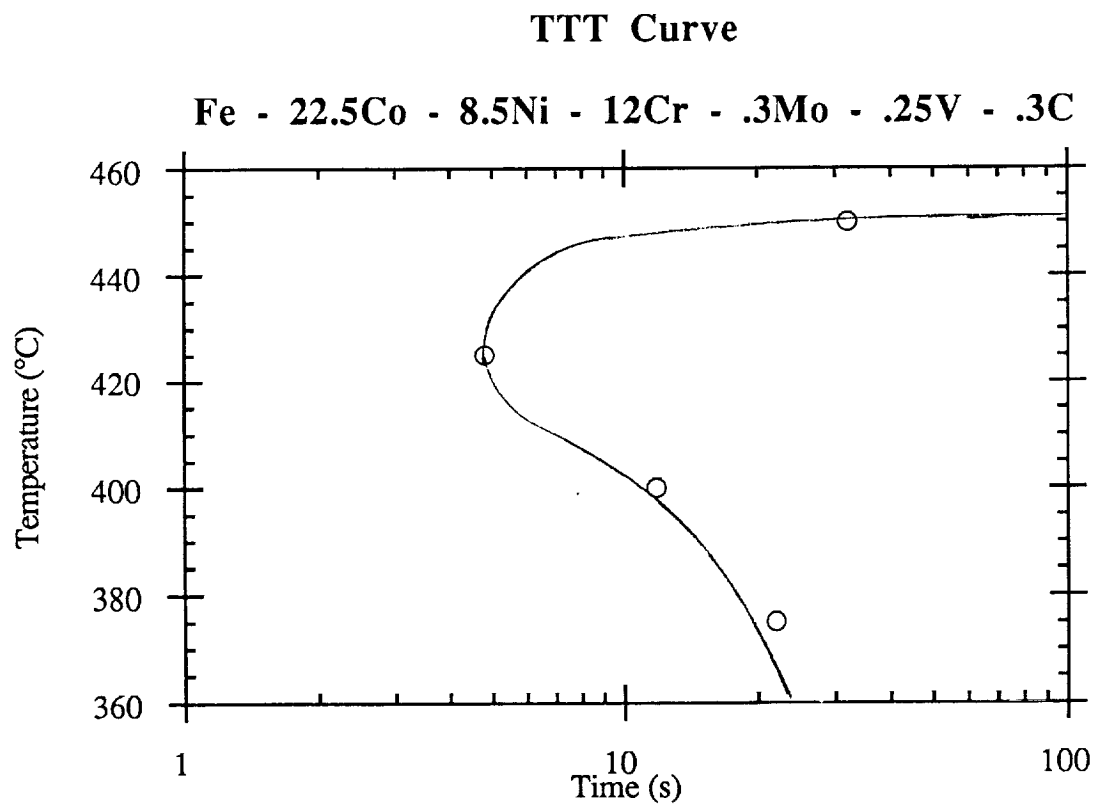
Fig. 9   Isothermal transformation start C-curve measured for prototype bearing steel in MMC Quenching Metallurgical Dilatometer after 1150C solution treatment.

strain-induced transformation with a yield strength of 79 ksi (547 MPa) and a UTS of 230 ksi (1590 MPa) limited by failure in the specimen threaded grip ends in association with the extreme strain hardening. Future tests will employ a smaller gage section diameter to compensate for the strain hardening. After deformation, the gage section was strongly magnetic indicative of martensitic transformation, and the martensitic microstructure produced is shown in Figure 11. Xray diffraction indicated a BCC volume fraction near 40%.

To achieve further transformation, the finely dispersed retained austenite can be destablized by draining its carbon via precipitation of Fe-based carbides in the martensite at tempering temperatures below the secondary hardening regime. The remaining austenite content in the strained material after temperi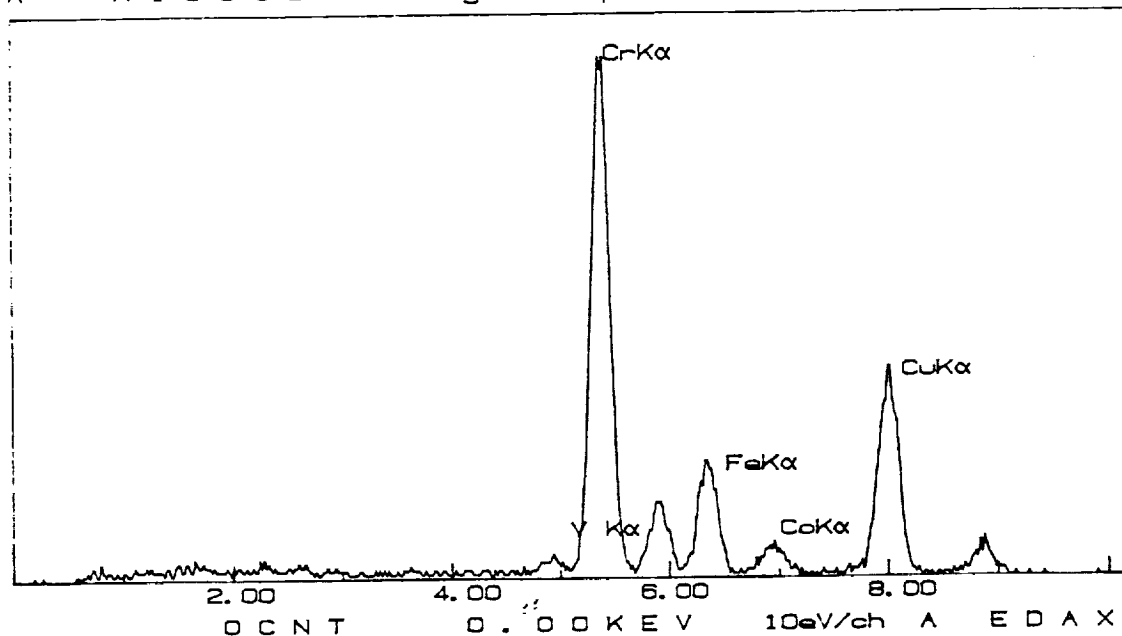ng 1 hr at 300-550C was determined by Xray diffraction and is plotted in Figure 12, with and without subsequent re-cooling to liquid nitrogen. Tempering at 300-500C decreases austenite content from its initial value after cryogenic deformation. The increase at 550C likely reflects austenite precipitation in the secondary hardening regime. Further transformation behavior during a second tensile deformation at liquid nitrogen temperature will next be investigated in material destabilized by tempering in the range of 300-450C. Tensile specimens will thus be strained twice at liquid nitrogen temperature with a tempering treatment applied between the two tests.

While the complicated processing being investigated is a long way from the originally intended single quench to room temperature, achieving a fully martensitic structure with full supersaturation of the alloy carbide forming elements by whatever means necessary will allow investigation of the carbide and austenite precipitation behavior which is essential to full characterization of the prototype alloy. Despite these difficulties, we remain encouraged that continuing basic model development together with full prototype evaluation will provide the needed information for greater accuracy in the next iteration of alloy design.

6. New Directions

Based on the results thusfar obtained on the prototype bearing steel, our highest priority modelling activity at present is the development of a sufficiently accurate martensite kinetics model to adequately control the M_s temperature in these unusual high alloy steels. While the basic mechanistic theoretical framework exists (22), the chief limitations to developing a comprehensive kinetic model have been remaining questions in the theory of solid solution strengthening in the presence of thermal activation (important to martensitic interfacial mobility), and the need to derive a database of kinetic parameters from the large amount of available kinetic data. Dr. Gautam

20
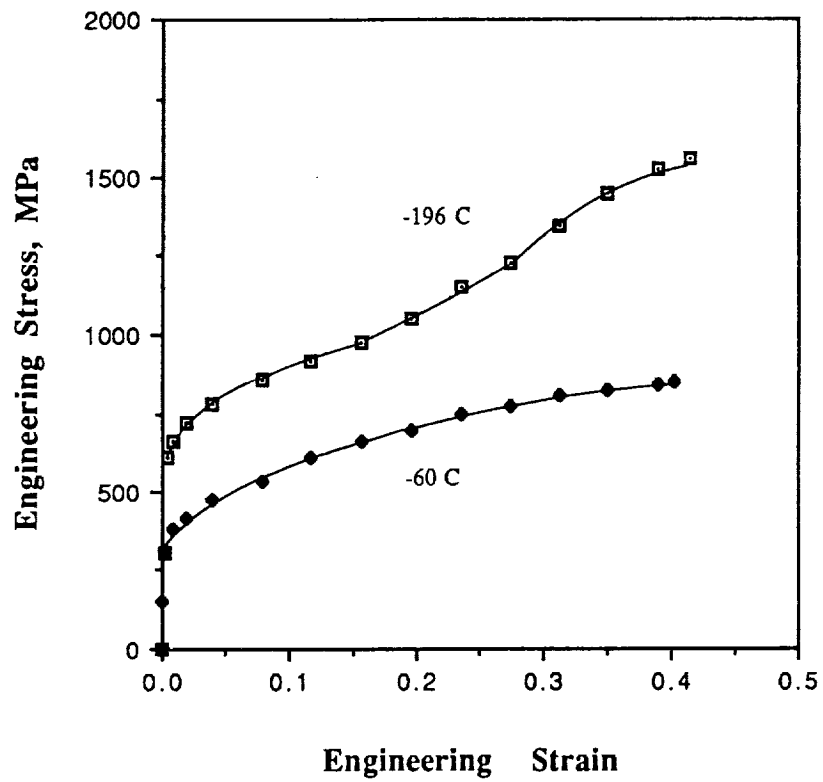
Fig. 10   Isothermal stress-strain curves of 1150C solution treated prototype bearing steel
measured at -60C and -196C.

100 μm
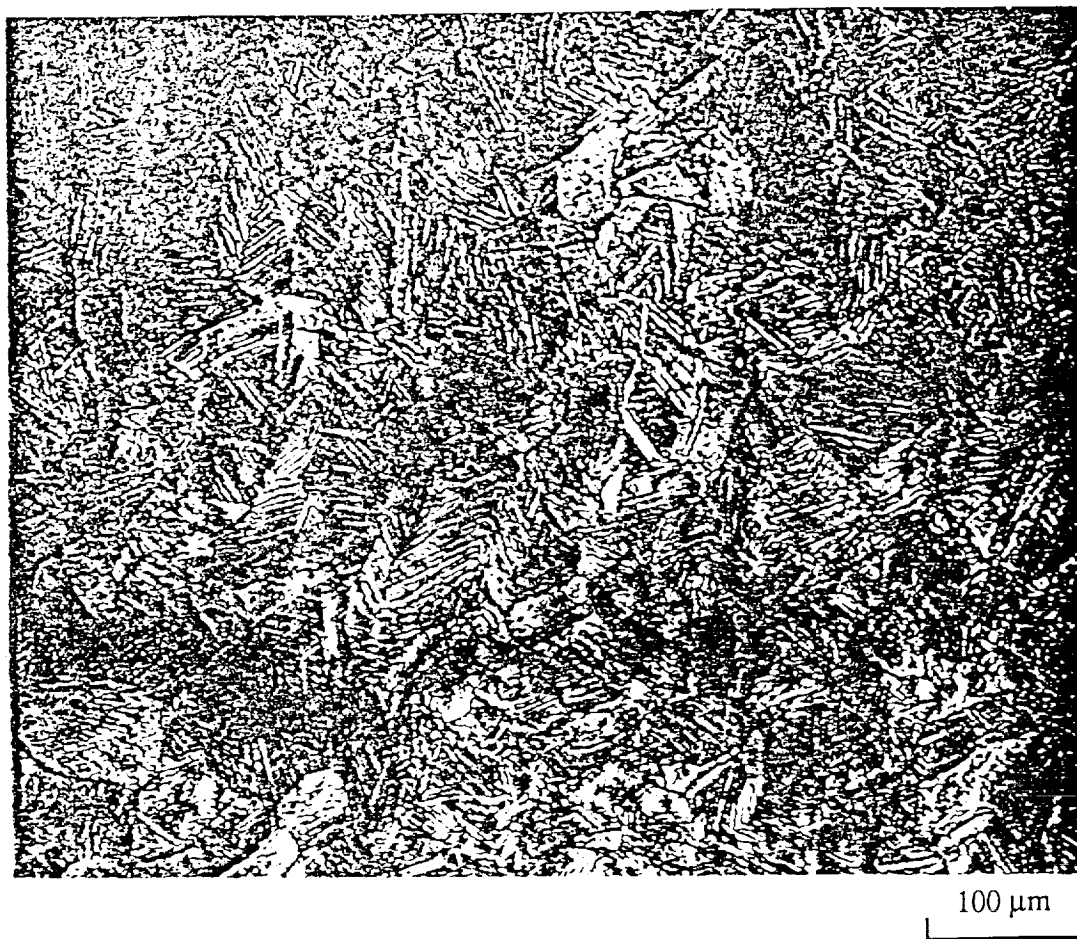
Fig. 11   Optical micrograph of strain-induced transformation microstructure after deformation at -196C.

volume fraction of austenite

$f_{v,\gamma}$
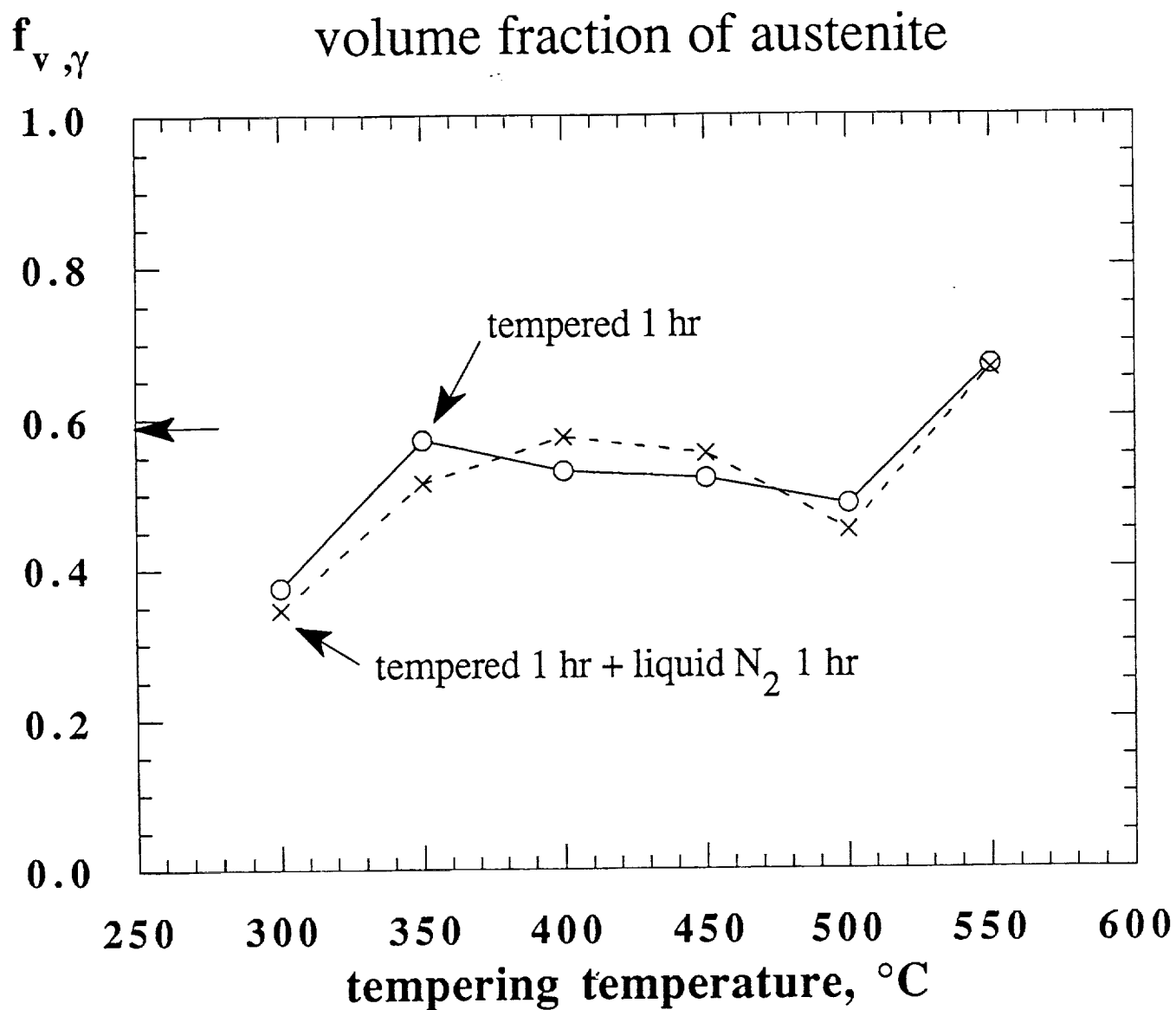
Fig. 12   Austenite content measured by X-ray diffraction after 1 hr tempering of prototype bearing steel deformed at -196C. Arrow indicates as-deformed austenite content. Also shown are values after subsequent cooling to -196C.

Ghosh is developing such a model incorporating a new theory of thermally activated solid solution strengthening (23-35) and employing literature kinetic data compiled from 35 references (12 from binary, 10 from ternary, and 2 from higher order Fe-based alloys). For barrierless heterogeneous martensitic nucleation with kinetics controlled by interfacial mobility, the critical driving force Δg_c defining the start of transformation can be expressed as (22):

$$\Delta g_c = -\left[\frac{2\gamma}{nd} + g_0 + w_f\right]$$

where γ is an interfacial energy, n is a nucleus thickness parameter defined by the nucleating defect potency, d is the close-packed interplanar spacing, g_0 is a strain energy parameter, and w_f is the frictional work of interfacial motion. Each term scales with the elastic modulus which is weakly composition and temperature dependent, but the interfacial work term w_f is strongly dependent on temperature, composition and imposed transformation rate through thermally activated solid solution strengthening. The nucleation-controlled transformation rate $\dot{f}$ can be expressed by

$$\dot{f} = \dot{f}_0 \exp(-Q/kT)$$

where the activation energy Q is related to w_f through an expression of the form

$$Q(w_f) = Q_0\left[1 - \left(\frac{w_f}{w_f^0}\right)^p\right]^q .$$

The new theory of solid solution strengthening (23-25) gives p = 1, q = 3/2 with $w_f^0 = 0.069\,(b/d)\mu\varepsilon^{4/3}c^{1/2}$ and $Q_0 = 2\mu\varepsilon^{2/3}c^{1/4}$, where b is a transformation partial dislocation Burgers vector, μ the shear modulus, ε the solute misfit strain, and c the solute concentration. Evaluating key parameters for each alloying element from transformation kinetic data and combining the elemental contributions to a root mean squared interaction force, these relations combine to specify Δg_c as a function of temperature, composition, and imposed transformation rate. A database of kinetic parameters so defined is currently being developed.

While the precise martensitic kinetic model is under development, a preliminary re-evaluation of the feasibility of our design concept has been undertaken in light of the observed transformation stability of the prototype alloy. An improved but still approximate constraint of the M_s temperature has been made attempting to hold the M_s at the same temperature (220C) as that of

the Aermet 100 alloy derivative of AF1410 recently developed at Carpenter Steel. Instead of constraining the T_o temperature, the martensitic transformation driving force Δg at 220C is held at its critical value ($\Delta g_c = -2100J/mole$) for transformation at this temperature in Aermet 100. Although this does not take full account of the composition dependence of Δg_c, it is calibrated to another high alloy steel of the same class. Furthermore, while the ThermoCalc alloy database is still employed for diffusional equilibria above 500C, the lower temperature thermodynamics governing martensitic transformation behavior is here evaluated using the Kaufman (Manlabs-NPL) database which has been more extensively applied to martensitic transformations previously.

The calculations indicate that the ability to maintain high alloy Ni content for cleavage resistance and to achieve high stability precipitated austenite is somewhat restricted by a saturation of the BCC stabilizing influence of Co near 20 wt. pct. A survey of additional BCC stabilizing solutes identified Al as particularly effective. This element is also of future interest for enhanced response to ion-nitriding in the development of case/core systems. Maintaining 0.3Mo-0.25V-0.30C from the previous analysis, Figure 13 presents calculation results for 9Cr and 12Cr steels with and without 0.5Al, showing (a) alloy Ni and Co contents for constant M_s, (b) stability of austenite precipitated at 510C expressed in terms of the transformation Δg at 300K, and (c) the equilibrium amount of austenite formed at 510C. Figure 14 shows the corresponding results with and without 1.0Al. Maintaining high Ni content in the alloy is promoted by lower Cr, higher Al, and Co near 20 wt. pct. Near this Co level the desired precipitated austenite stability of $\Delta g = 1500$ - 2000 J/mole can be achieved with Al between 0.5 and 1.0 wt. pct. with a reasonable austenite amount of 15 to 20 pct. Lowering Cr. to 9 wt. pct. appears desirable and Al additions will help to compensate decreased oxidation resistance. Al solubility limits are being addressed by an assessment of the thermodynamics of the β'-NiAl compound.

Overall, the analysis incorporating a more realistic treatment of austenite stability indicates the concept of combining precipitated austenite transformation toughening with secondary hardening in a high Co martensitic stainless is still quite feasible. Detailed design calculations will be undertaken once the improved martensite kinetic model is available and the first prototype steel has been fully evaluated.

It should be noted that achieving a high stability precipitated austenite dispersion while maintaining a high M_s temperature represents conflicting thermodynamic objectives, and the high M_s constraint limits allowable levels of Cr and Ni, otherwise desired for corrosion resistance and toughness. As an alternative to a quench hardening steel, our experience with the prototype alloy raises the possibility of a more stable alloy based on strain-induced martensitic transformation via

Fe-Co-Ni-Cr-Al-.3Mo-.25V-.3C
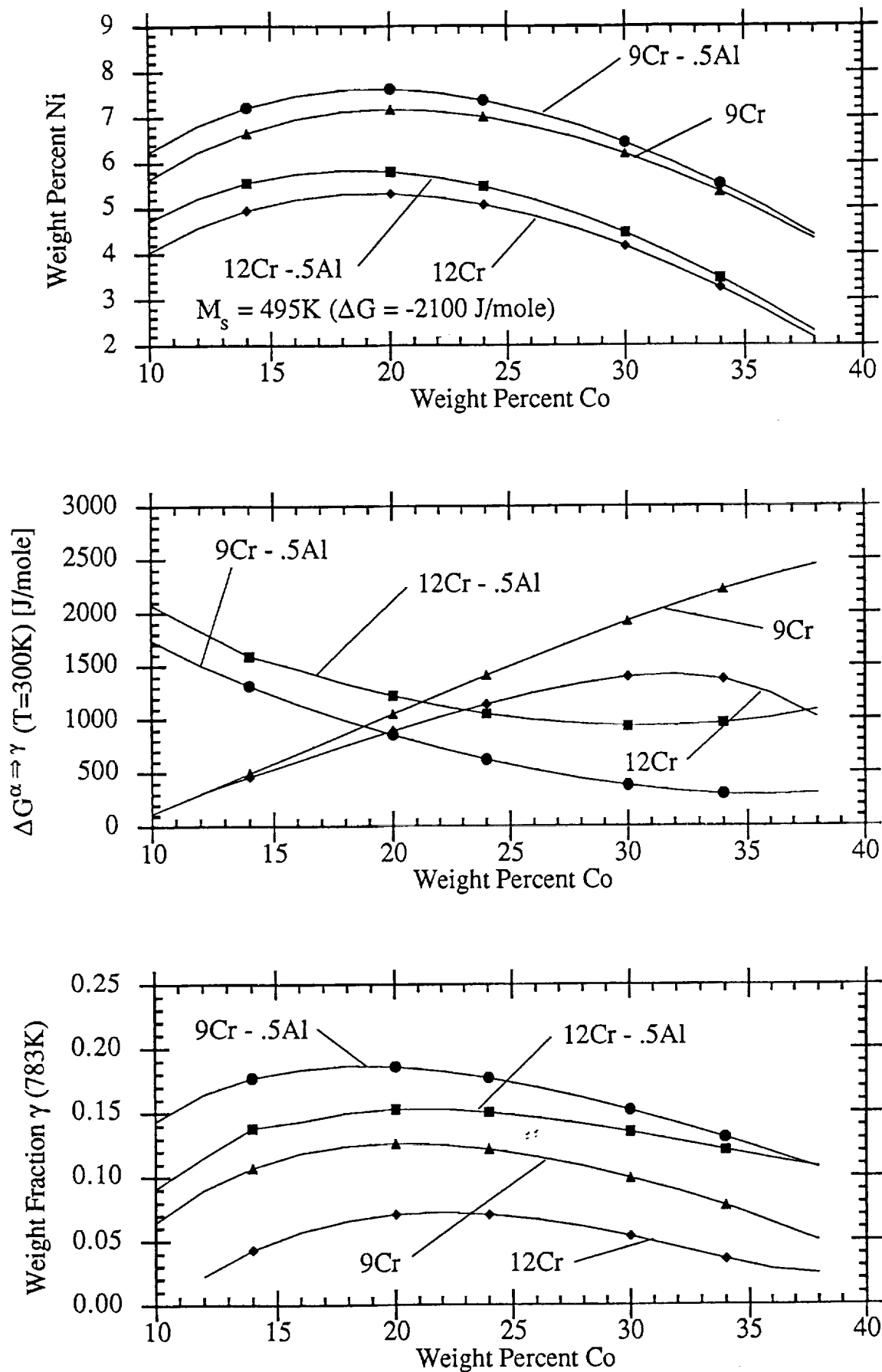
Fig. 13   Computed alloy compositions for constant M_S of 220C, with corresponding stability (ΔG at 300K) and amount of precipitated austenite at 510C for 12Cr and 9Cr alloys with and without 0.5Al.

Fe-Co-Ni-Cr-Al-.3Mo-.25V-.3C
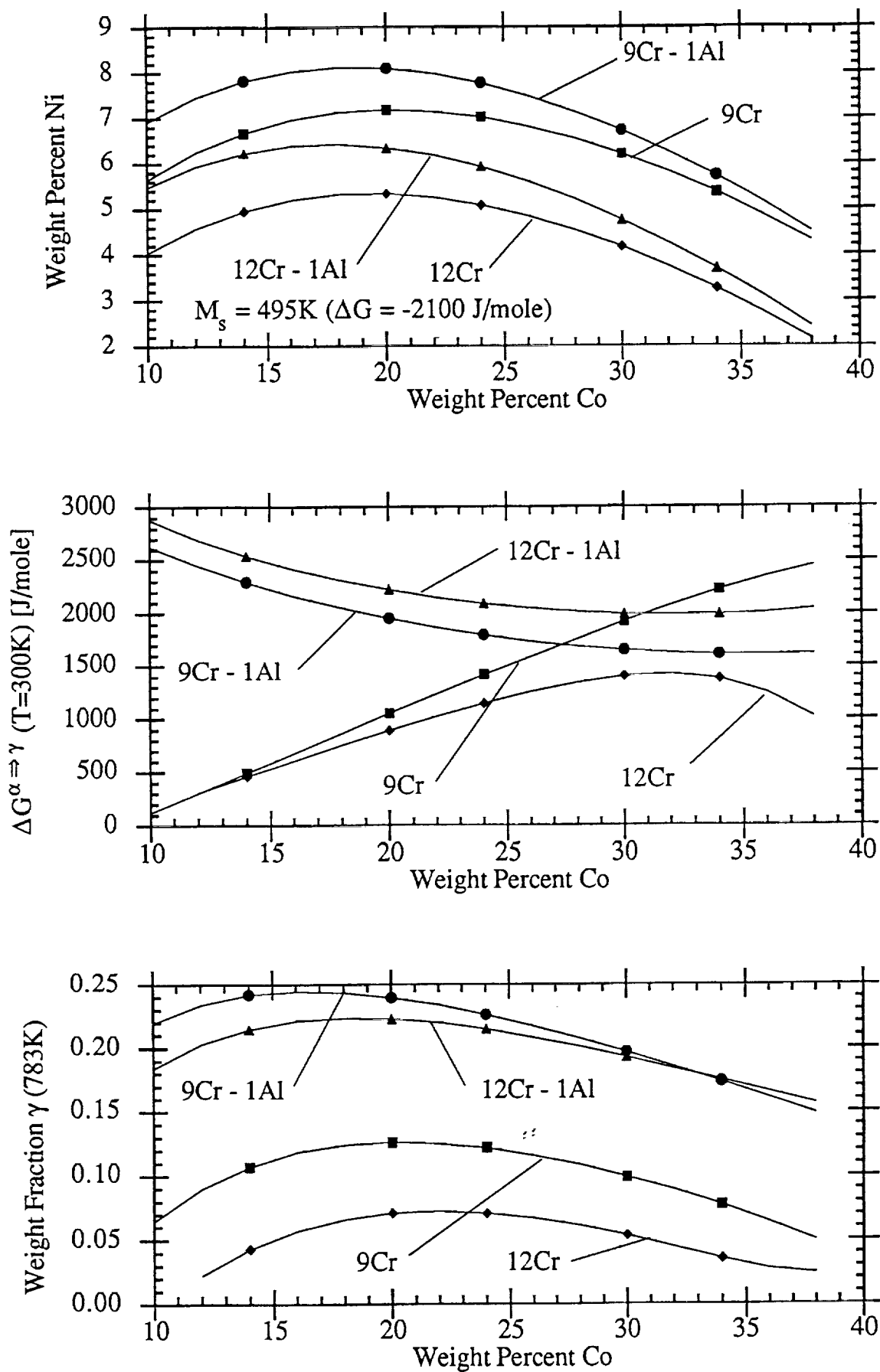
Fig. 14   Computed alloy compositions and precipitated austenite characteristics for 9Cr and 12Cr alloys of Fig. 13 with and without 1.0Al.

cryogenic forming. Although the approach requires more complicated processing, it may allow compositions capable of higher toughness levels, particularly at cryogenic temperatures. As a project topic for a Masters in Manufacturing degree program, Anatol Bilyk, who studied the prototype alloy as a Senior project, is proposing to evaluate the fabrication of bearing races from the prototype steel by a series of cryogenic mandrel expansion steps with intermediate tempering treatments. This may open a promising additional direction for our design efforts.

7. REFERENCES

(*denotes papers acknowledging NASA support)

* 1. G. B. Olson, "Materials Design:An Undergraduate Course," to appear in <u>Morris E. Fine Symposium</u>, TMS–AIME, Warrendale, Pensylvania, in press.

* 2. G. B. Olson, "New Steels by Design," <u>J. Materials Ed.</u>, in press.

* 3. G. B. Olson, "Science of Steel," in <u>Innovations in Ultrahigh–Strength Steel Technology</u>, eds. G. B. Olson, M. Azrin, and E. S. Wright, Sagamore Army Materials Research Conference Proceedings:34th (1990) p. 3.

* 4. G. B. Olson, M. Azrin, and E. S. Wright, eds., <u>Innovations in Ultrahigh–Strength Steel Technology</u>, Sagamore Army Materials Research Conference Proceedings: 34th (1990).

5. R. Wagner and R. Kampmann, in <u>Innovations in Ultrahigh–Strength Steel Technology</u>, eds. G. B. Olson, M. Azrin, and E. S. Wright, Sagamore Army Materials Research Conference Proceedings:34th (1990) p. 209.

6. K–U. C. King, "The Eigenstrain Method:Extension to Lattice Theory and Application to Coherent Precipitation," Ph.D. thesis, Northwestern University, June 1990.

7. J. S. Montgomery, doctoral research in progress, Northwestern University.

8. G. R. Speich, in <u>Innovations in Ultrahigh–Strength Steel Technology</u>, eds. G. B. Olson, M. Azrin, and E. S. Wright, Sagamore Army Materials Research Conference Proceedings:34th (1990) p. 89.

9. H. M. Lee, S. M. Allen, and M. Grujicic, in <u>Innovations in Ultrahigh–Strength Steel Technology</u>, eds. G. B. Olson, M. Azrin, and E. S. Wright, Sagamore Army Materials Research Conference Proceedings:34th (1990) p. 127.

10. H. M. Lee, "Stability and Coarsening Resistance of M_2C Carbides in the Secondary Hardening Reaction," Ph.D. thesis, MIT, February 1989.

11. G. Ghosh and G. B. Olson, Northwestern University research in progress.

12. A. Needleman, in <u>Innovations in Ultrahigh–Strength Steel Technology</u>, eds. G. B. Olson, M. Azrin, and E. S. Wright, Sagamore Army Materials Research Conference Proceedings:34th (1990) p. 331.

13. M. J. Gore, G. B. Olson, and M. Cohen, in <u>Innovations in Ultrahigh–Strength Steel Technology</u>, eds. G. B. Olson, M. Azrin, and E. S. Wright, Sagamore Army Materials Research Conference Proceedings:34th (1990) p. 407.

14. M. L. Schmidt and M. J. Gore, in <u>Innovations in Ultrahigh–Strength Steel Technology</u>, eds. G. B. Olson, M. Azrin, and E. S. Wright, Sagamore Army Materials Research Conference Proceedings:34th (1990) p. 407.

15. F. Stavehaug, "Transformation Toughening of Γ'–Strengthened Metastable Austenitic Steels," Ph.D. thesis, MIT, June 1990.

16. G. N. Haidemenopoulos, G. B. Olson, and M. Cohen, <u>Innovations in Ultrahigh-Strength Steel Technology</u>, eds. G. B. Olson, M. Azrin, and E. S. Wright, Sagamore Army Materials Research Conference Proceedings:34th (1990) p. 549.

17. C. Kuehmann and G. B. Olson, Northwestern University research in progress.

18. P. M. Anderson, J. S. Wang, and J. R. Rice, in <u>Innovations in Ultrahigh-Strength Steel Technology</u>, eds. G. B. Olson, M. Azrin, and E. S. Wright, Sagamore Army Materials Research Conference Proceedings:34th (1990) p. 619.

19. G. L. Krasko, C. Li, R. Wu, A. J. Freeman, and G. B. Olson, Northwestern University research in progress.

20. J. F. Watton, G. B. Olson, and M. Cohen, in <u>Innovations in Ultrahigh-Strength Steel Technology</u>, eds. G. B. Olson, M. Azrin, and E. S. Wright, Sagamore Army Materials Research Conference Proceedings:34th (1990) p. 705.

21. J. H. Graves and A. A. Anctil, MTL research in progress.

22. G. B. Olson and M. Cohen, "Dislocation Theory of Martensitic Transformations," in <u>Dislocations in Solids</u>, Vol. 7, Chapter 37, ed. F. R. N. Nabarro, North Holland, Amsterdam (1986) p. 295.

23. R. J. Arsenault, S. Patu, and D. M. Esterling, <u>Metall. Trans.</u>, <u>20A</u>, (1989) 1411.

24. R. J. Arsenault, S. Patu, and D. M. Esterling, <u>Metall. Trans.</u>, <u>20A</u>, (1989) 1419.

25. R. J. Arsenault and S. Li, <u>Metall. Trans.</u>, <u>20A</u>, (1989) 1429.

APPENDIX A

Materials Design: An Undergraduate Course

MATERIALS DESIGN:
AN UNDERGRADUATE COURSE

G.B. Olson
Northwestern University
Department of Materials Science and Engineering
Evanston, Illinois 60208

Abstract

General principles of systems engineering are applied to the design of materials to meet specific performance objectives. Results of ongoing research on processing/structure and structure/property relations in ultrahigh-strength steels are used to illustrate the formulation of quantitative microstructural objectives to achieve required property combinations, and the computer thermodynamics-based design of compositions responding to prescribed processing conditions. A class project addresses the conceptual design of a 7-component stainless bearing steel for a critical Space Shuttle application.

Introduction

On the suggestion of Professor Morris Fine, this paper, rather than presenting the usual discussion of research results, will instead focus on teaching and its interrelation with research. In the late 1960's and early 1970's, Professor Fine taught a pioneering course at Northwestern on Materials Development which in part responded to the concerns of accreditation boards regarding the declining design component of engineering undergraduate curricula. Twenty years later, the concerns are more valid than ever. In the spirit of Professor Fine's innovations, a new course at Northwestern (1) directly addressing Materials Design has been made possible by a multi-institutional research program; centered at Northwestern, the interdisciplinary Steel Research Group (SRG) program focusses on the quantitative scientific principles allowing design of new classes of advanced steels.

To approach materials design in the broadest context, a survey of instructors of Systems Engineering courses at Northwestern identified a concise review of the systems approach by G.M. Jenkins (2), presenting an excellent overview that could be readily translated to materials problems. A recent review by Ashby (3) effectively describes the process of materials selection in the various stages of engineering design, and provides an excellent framework for the specification of material property objectives to achieve desired performance. To provide materials science students with sufficiently quantitative design tools, computer laboratory sessions were found effective in developing proficiency in available thermodynamic and kinetic software, most notably the ThermoCalc system (4) that has formed the cornerstone of our materials design research. Applications to control of both constrained equilibria and thermodynamics-based kinetic scaling factors provided the basis of student team design projects during the second half of the course.

Materials as Systems

The central paradigm of materials science is the sequential interrelation of processing, structure, properties, and performance as depicted in the linear structure of Figure 1. While the notion of materials as systems has been well developed by Cyril Smith (5) in the context of material *structure* as a hierarchy of interacting microstructural subsystems, the concept can be further broadened to regard each of the blocks of Figure 1 as a primary subsystem, each of which can itself be further subdivided into a hierarchy of interacting subsystems. Although "cause and effect" logic suggests a sequence of interrelations from left to
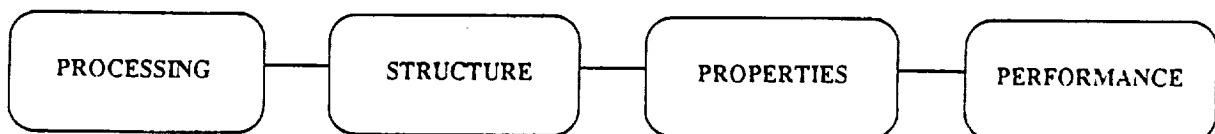

Figure 1: Linear structure of materials science, defining primary material subsystems.
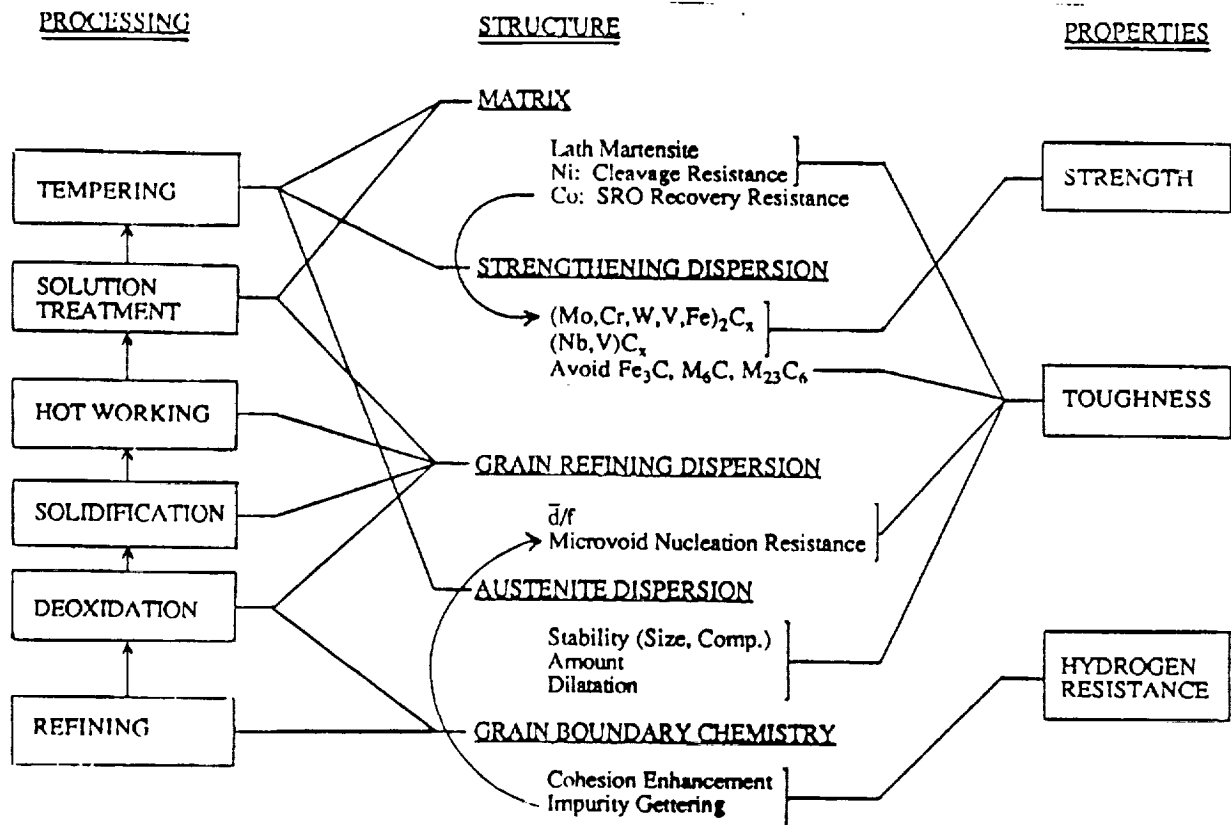
Figure 2: Flow-block diagram illustrating the structure of Co-Ni secondary hardening steels as a system.

right in Figure 1 (e.g. structure controls properties), Morris Cohen (6,7) has observed there is a "reciprocity" whereby it is equally valid to regard our perception of *structure* as controlled by the *properties* we wish to explain. This reciprocal view is particularly useful in materials design.

As outlined by Jenkins (2) a system in general is a complex grouping of components which is divisible into a hierarchy of interacting subsystems, usefully represented by a flow-block diagram. Figure 2 illustrates such a diagram, expanded from the general structure of Figure 1, representing the ultrahigh-strength martensitic alloy steels addressed by the SRG research program. Shown are the key microstructural subsystems controlling the three primary properties of interest, together with the stages (subsystems) of processing affecting each. While further details will be discussed later, it is evident from Figure 2 that in addition to the horizontal primary subsystem interactions reflected in Figure 1, important vertical subsystem interactions also exist such as the effect of recovery resistance on carbide precipitation, and the effect of impurity gettering on microvoid nucleation resistance. As is also a universal feature of systems, the material of Figure 2 is part of a hierarchy of larger systems, strongly influenced by higher levels, particularly in the formulation of its objectives. It is the application of the steel as a load-bearing component

in an engineering structure that defines its performance objective quantifying the required three primary properties of strength, toughness, and hydrogen resistance. Further, as for all systems, the ultimate system objective of a *combination* of properties demands a compromise between conflicting objectives of property subsystems (e.g. strength vs. toughness), and to function at maximum efficiency the system must be *designed*.

Systems Design of Materials

Stages of Systems Engineering

The sequential stages of the general systems design approach described by Jenkins (2) are depicted in Figure 3. We here briefly examine each of these in the context of materials.

Analysis

The basic steps of systems analysis consist of problem formulation, definition of the system and the wider system in which it functions, and definition of the system objectives. In the case of materials, problem formulation consists of identification of a broad materials performance need. The materials system is then defined in terms of class of material and microstructure, and important subsystems and
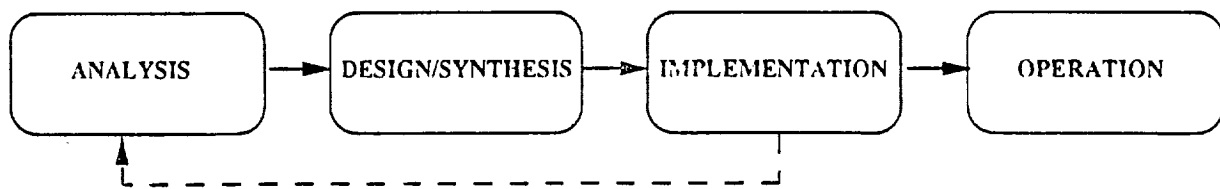
Figure 3: Stages of systems engineering (2).

interactions are identified and represented in a flow-block diagram as in Figure 2. While Figure 2 reflects a fairly advanced stage of analysis, an initial stage would emphasize simplicity and flexibility of approach. Consideration of the wider system then defines the function of the material in a device, which in turn prescribes performance requirements.

The manner in which property/performance relations can be used to set quantitative property objectives for a material is well described in the review by Ashby (3). Using the examples of table legs, bicycle forks, springs, and pressure vessels, a series of combined property parameters superimposed on property cross-plots is used to compare competing materials. Such an analysis is not only useful to the design engineer selecting materials from those available, but also serves to define property objectives for the materials scientist designing an improved material to better compete with available alternative materials. For the ultrahigh strength steels of Figure 2, property objectives were defined by choosing a significant strength increment beyond that which can be reliably used in current commercial steels for advanced structural applications such as aircraft landing gear. This defines an ultimate tensile strength range of 2000-2400 MPa corresponding to a hardness of R_c55 to 60. Quantitative K_{IC} toughness objectives are then defined by the toughness/strength ratio required for a desired minimum critical flaw size. Hydrogen resistance, quantified in these steels by the stress corrosion threshold K_{ISCC}, is then specified by a desired minimum K_{ISCC}/K_{IC} ratio.

Another important early step in analysis is the organization of an interdisciplinary design team for which Jenkins (2) gives useful general guidelines. It is particularly noteworthy that the required breath of knowledge demands that the materials design team leader must be a materials scientist, but necessarily one well suited to interaction with related disciplines.

Design/Synthesis

The first step in the synthesis of understanding in design is modelling. Ideally, quantitative models should be developed for each of the important structure/property and property/structure relations depicted in Figure 2, spanning a hierarchy of structural scales. While empiricism at some level is inevitable,

the most useful models, particularly for the generally nonlinear phenomena at play in materials, are as fundamentally mechanistic as possible. Jenkins (2) cautions however, that modelling for design must be purposeful, with the goal of optimization rather than subsuming facts. In this regard it is useful to prioritize phenomena and decide the necessary accuracy of required models.

It should perhaps be acknowledged at this point that materials science is a relatively young field for which quantitative models are not abundant. Even in the most scientifically advanced area of high strength steels, relations for toughness and hydrogen resistance remain quite qualitative. The kinetic theory of phase transformations has provided a reasonably quantitative basis for the microstructural evolution underlying process/structure relations, however, and recent progress indicates that quantitative microstructural objectives can be formulated and achieved to provide specified strength with desired qualitative changes in toughness and hydrogen resistance (8,9).

The second stage of synthesis is the actual application of models in simulation of material behavior on both the local scale of microstructural subsystems and ultimately the global scale of the entire system. Simulation is then applied to system optimization. As emphasized by Jenkins (2) it is here crucial to avoid "sub-optimization" whereby a subsystem is optimized at the expense of the total system. The total system must be optimized as a whole, recognizing constraints imposed by competing subsystems. Again material performance demands a combination of properties, such that major increases in one property can be useless if other necessary properties are degraded.

Another important aspect of system optimization is the application of simulations to the identification of sensitive variables (in material composition and processing) in order to minimize sensitivity for controllability; i.e. "sharp" optima are to be avoided. Control and reliability also demand that control systems be built into the design, ideally allowing for process monitoring and readjustment. Reliability also requires some tolerance for the unpredictable, such that statistical variations can not cause an excessive fraction of processed material to fall below final specifications.

Implementation and Operation

As depicted in Figure 3, the next step in systems engineering is *implementation*, which here corresponds to the production of a prototype material. The testing of model predictions via characterization of prototypes allows refinement of the system models through an iterative process denoted by the dashed line in the figure.

When sufficient optimization is achieved, the *operation* stage is entered corresponding to the setting of materials specifications in terms of composition and processing.

It should be recognized at this point that the actual practice by which new materials are currently developed consists of the simultaneous evaluation of a set of materials with variations in composition and processing to allow optimization via empirical process/ structure correlations with minimal involvement of structural details. Experience in other engineering systems would strongly indicate that, once mechanistic models are sufficiently mature, the true design of materials through the deliberate approach of Figures 2 and 3, involving the sequential characterization of a small number of prototype materials, will ultimately lead to greater and more rapid advances. The general principles reviewed here offer a glimpse of the future of materials design. Recent progress suggests that, for steels at least, that future may be close at hand.

The Example of Ultrahigh-Strength Steels

Specific examples giving meaning to the development and application of mechanistic models for design just discussed are obtained from results of SRG research on ultrahigh-strength martensitic steels. Detailed theoretical and experimental results defining process/structure and structure/property relations for each of the microstructural subsystems listed in Figure 2 are reviewed elsewhere (8,9). Examples concerning behavior of the alloy matrix include the electronic basis of Ni-enhancement of cleavage resistance (10) and the mechanism of Co-enhancement of dislocation recovery resistance (9). We will here highlight advances in the mechanistic modelling of these subsystems, emphasizing examples which serve to illustrate key points.

Control of competing precipitation reactions in secondary hardening martensitic steels offers an excellent example of quantitative processing/ structure relations. Achieving optimum strength/toughness combinations in these steels requires near completion of M_2C alloy carbide precipitation to eliminate Fe-base Fe_3C carbides which precipitate earlier in a coarse form limiting toughness through microvoid nucleation (11). Completion results in an overaged microstructure where strength is controlled by the Orowan bypass mechanism. In this regime M_2C particle size refinement governs strengthening. Hence the desired microstructural objectives is to achieve the finest particle size at completions of precipitation. Extensive study (9) of M_2C precipitation behavior by a range or experimental techniques in the 14Co-10Ni steel AF1410 shows nucleation and coarsening behavior with suppressed growth consistent with theory of precipitation at high supersaturations (12), and shows a particle composition trajectory indicative of coherent precipitation. The primary size scaling factor in the high supersaturation regime is the initial critical nucleus size which scales inversely with the driving force for coherent precipitation. Incorporating the elastic contribution of particle coherency, the latter can be computed as a function of alloy composition using the ThermoCalc software and database. However, an important constraint enters because the M_2C phase is typically metastable, and completion of its precipitation must be achieved before the embrittling incoherent interfacial precipitation of equilibrium carbides such as M_6C. Toward design of optimal alloy compositions for strength/toughness, Figure 4 depicts computed contours of precipitation driving force for (a) the M_6C carbide and (b) the coherent M_2C carbide, as functions of Cr and Mo content in 14Co-10Ni-0.25C steels (13). Experience from experimental alloys with Cr and Mo contents along the dashed line in Figure 4a indicates interfacial embrittlement during secondary hardening for M_6C driving forces beyond 15 kJ/mole. This then provides the constraint that alloy composition must lie to the left of the dashed curve superimposed in Figure 4b. Subject to this constraint, maximizing the coherent M_2C driving force for efficient strengthening defines the alloy composition denoted by the open point. This point lies very close to a recently developed alloy with excellent strength/toughness properties (14).

An example of analysis of structure/property relations involving interdisciplinary collaboration with applied mechanics, introducing materials science students to the capabilities of numerical finite-element methods, is the investigation of the role of particle dispersion geometry on microvoid nucleation resistance. Once unnecessary particles such as Fe_3C are eliminated by optimal processing, the microvoid nucleation resistance governing ductile fracture toughness becomes controlled by the grain refining dispersion necessary to limit grain coarsening during solution treatment. The geometric requirements in terms of particle diameter d and volume fraction f for grain refinement are well established. Combining this with the predicted role of these variables from the numerical modelling of microvoid nucleation (15) has allowed an assessment of the toughening benefits of particle size refinement while maintaining a fixed grain size (9). Dispersions
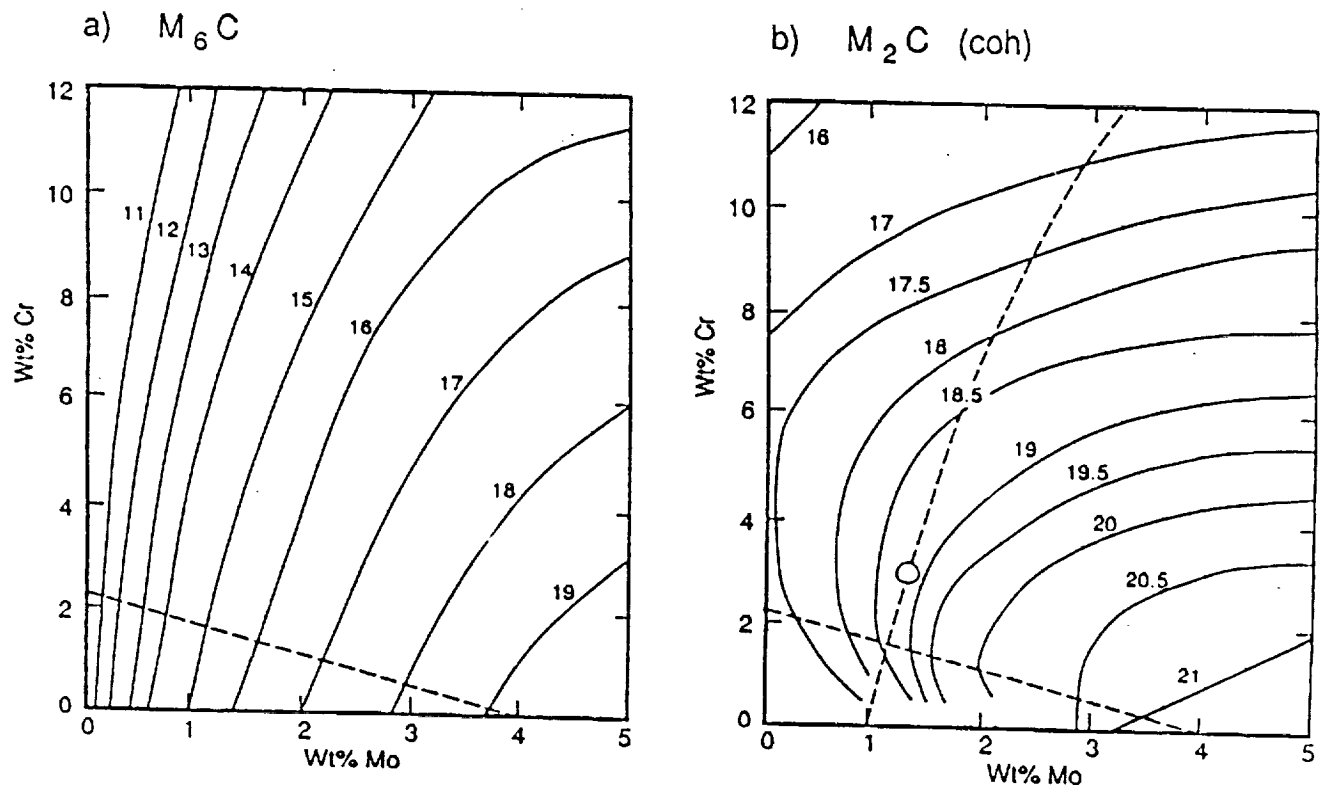
a) M_6C

b) M_2C (coh)

Figure 4: Computed precipitation driving force (kJ/mole) at 510C for alloys containing 14Co-10Ni-0.25C. (a) incoherent M_6C, (b) coherent M_2C (13).

with the desired finer size and required coarsening resistance may be achievable by rapid solidification processing.

A unique example of a structure/property relation amenable to rather direct control through thermodynamics is the transformation toughening from a dispersion of precipitated austenite. Experiments in model austenitic steels identify the optimal thermodynamic stability for maximum transformation toughening and isolate the important role of transformation dilatation (9). Transformation kinetic theory predicts the roles of particle composition and size on the transformation stability of dispersed austenite, and experiments employing multi-step heat treatments in AF1410 steel demonstrate the toughening benefit of optimal stability austenite dispersions (16). Constrained equilibrium calculations employing ThermoCalc predict the amount, composition, and thermodynamic stability of austenite that can be precipitated during secondary hardening treatment, and models for the composition dependence of the austenite and martensite lattice parameters can allow prediction of alloy compositions for increased transformation dilatation for enhanced toughening.

Our best example of an interdisciplinary approach to a structure/property relation involving collaboration of metallurgy, mechanics, and quantum physics explores

the ultimate electronic origin of intergranular cohesion underlying the hydrogen resistance of ultrahigh strength steels. Intergranular hydrogen stress corrosion in these steels is invariably associated with prior interfacial segregation of impurities which reduce intergranular cohesion (17). Modelling the thermodynamics and mechanics of the competition between crack-tip blunting and brittle interfacial separation has predicted a correlation between the embrittling potency of a segregant (including hydrogen) and the difference between the free energy of segregation to grain boundaries and free surfaces, consistent with available data (18). The resulting thermodynamic description of embrittlement gives a well defined physics problem being addressed by total energy electronic calculations employing suitable models of grain boundary and free surface atomic structures (9,19,20). While these calculations are only now revealing features of electronic structures which correlate with the thermodynamic quantities underlying embrittlement, and have yet to reveal new principles of interfacial cohesion enhancement, the approach introduces materials students to the capabilities of total electronic calculations, illustrates the manner in which materials-related problems can be formulated to be addressed by allied disciplines, and emphasizes the effectiveness of thermodynamics as a medium of communication across disciplines.

A more direct means of applying thermodynamics to the improvement of hydrogen resistance, while providing an example of composition design for optimal process interactions, is the design of novel gettering compounds to remove embrittling residual impurities such as phosphorus from grain boundaries (21). A thermodynamic survey identified lanthanum phosphate as potentially the most stable gettering phase for phosphorus in steels, and further calculations indicated the metastable phase could be accessible at high melt undercooling achievable by rapid solidification. Preliminary rapid solidification experiments performed on a simple NiMo steel confirmed formation of such a phase and revealed a major improvement in hydrogen stress corrosion resistance as represented by K_{ISCC}. The fine coarsening resistant dispersion of the stable compound further provides stable grain refinement at relatively high solution treatment temperatures.

Class Project: Design of a Stainless Bearing Steel

From the viewpoint of undergraduate materials students, research examples just cited serve to not only convey an important sense of the nature of interdisciplinary research for purposeful modelling, but many of the final outputs of these activities are expressible in terms of undergraduate thermodynamics and kinetics, yielding principles compatible with the available tools of the ThermoCalc system. These then provided the basis for student design projects, the most intricate example of which was a team project directed at a stainless bearing steel for the Space Shuttle Main Engine (SSME) turbopumps (22).

Mechanical property objectives adopted for this demanding application of a martensitic stainless steel were a minimum hardness level of R_c60 for wear and fatigue resistance, with a doubling of K_{IC} and K_{ISCC} relative to the 440C alloy steel currently employed, in order to achieve the desired level of reliability. Applying the approach represented in Figures 2 and 3, composition was first constrained by available knowledge (17) of alloying effects on intergranular cohesion (primarily excluding Mn and Si) and compatibility with rapid solidification and lanthanum treatment for impurity gettering and stable grain refinement. Matrix composition was then constrained to include 12Cr for stainless properties. Applying an Orowan strengthening analysis to available dispersion hardening data from experimental high-Co secondary hardening steels, (9), a minimum carbon level of 0.30 wt.pct. was estimated to achieve the desired R_c60 hardness in this class of alloy. A rough initial estimate of Mo content of 1.0 wt.pct. was then adopted, based on previous results such as those of Figure 4.
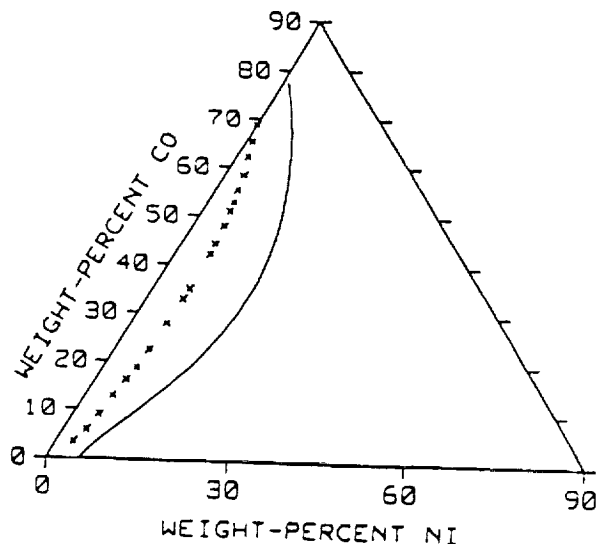

Figure 5: Composition diagram for 12Cr-1Mo-0.3C steels representing Co and Ni contents giving equal FCC and BCC free energies at $T_o = 940K$. Solid line is equilibrium FCC/FCC+BCC phase boundary (22).

At this point, an approximate constraint was introduced to maintain a sufficiently high martensitic transformations temperature (Ms) to achieve the desired lath martensitic microstructure. Lacking suitable martensitic kinetic parameters for the high alloy range of interest, the FCC-BCC To partitionless equilibrium temperature was set equal to that of AF1410 steel (940K). This then defined the range of alloy Ni and Co contents represented by the X-curve in Figure 5. A unique Ni and Co content along this line was then selected by consideration of the amount and stability of austenite that could precipitate at secondary hardening temperatures near 500C for subsequent transformation toughening in service at and below room temperature. Stability was assessed by the FCC-BCC free energy difference at room temperature and set slightly higher than the optimally stable dispersed austenite studied in AF1410. This stability level could be achieved with a total austenite amount of 20 pct. A secondary objective was to maintain a high Ni content in the BCC matrix for cleavage resistance.

Optimization of carbide forming elements was then examined employing driving force calculations like those of Figure 4, holding Cr at 12 wt.pct. and varying Mo and V. For this high Cr content the M_6C driving force was easily maintained below the critical level of Figure 4. The driving force for $M_{23}C_6$ was
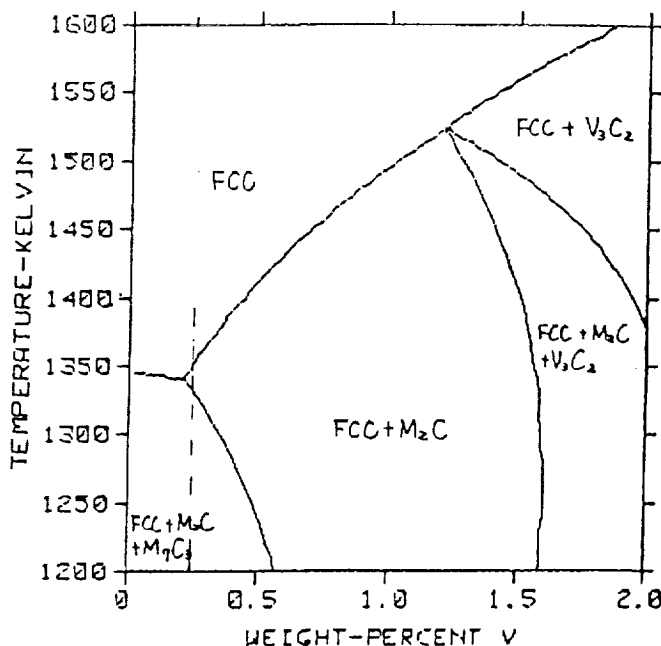
Figure 6: Phase diagram section vs. V content for Fe-30Co-12Cr-6Ni-0.3Mo-0.3C (22).

significantly higher but corresponding experimental information regarding embrittlement behavior associated with this carbide is currently lacking, thus identifying a need for further experiment. In this range of composition, the coherent thermodynamic model prediction of the driving force for the desired coherent M_2C was rather insensitive to Mo content, but strongly increased with V as desired for particle size refinement for efficient strengthening. Maintaining a Mo level of 0.3 wt.pct. to provide pitting corrosion resistance, the V level was then set by considering solution treatment requirements defined by the computed phase diagram section of Figure 6. A selected level of 0.25 wt.pct. corresponds to the onset of a steep rise in solution temperature with further increase of V. The final alloy composition thus defined can be solution treated at 1100C where the grain refining dispersions formed by rapid solidification should remain quite stable.

By this sequence of thermodynamic calculations, a unique 7-component alloy composition has been defined which is predicted to be thermodynamically capable of generating the desired set of microstructural features defined in Figure 2 under fairly well prescribed conditions of solidification, solution treatment, and tempering. Following a second iteration of the calculational sequence for improved self consistency, a prototype of such an alloy has been prepared and is currently being evaluated under NASA sponsorship.

Closure

A systems approach to materials design has been outlined based on general principles of systems engineering. Employing quantitative relations developed from ongoing research on ultrahigh-strength steels, the feasibility of computer-aided thermodynamics-based design of alloy compositions capable of achieving prescribed microstructural objectives under specified processing conditions has been demonstrated with the conceptual design of a stainless bearing steel uniquely combining a set of phenomena with high potential for substantial property improvements.

It is noteworthy that, while the ongoing research program made a materials design course possible, the scheduling of the course greatly catalyzed the process of integrating results within a well-defined design approach, and profoundly altered the direction of the research program. The first complete materials design exercises occurred in fact in the class projects. This synergism between teaching and research provided an exhilarating experience for all who participated in it.

References

1.   Materials Design, Northwestern University course MSc-C95, Spring Quarter, 1989.

2.   G.M. Jenkins, "The Systems Approach," in Systems Behavior, ed. J. Beishon and G. Peters, Open University Press, 1972.

3.   M.F. Ashby, "Materials Selection in Conceptual Design," in Ashby Symposium on Materials Design ed. D. Embury, ASM, Metals Park, Ohio (1989).

4.   B. Sundman, B. Jansson, and J.O. Andersson, CALPHAD, 9 (1985) 153.

5.   C.S. Smith, A Search for Structure, MIT Press, Cambridge, MA, 1981.

6. M. Cohen, "Unknowables in the Essence of Materials Science and Engineering," Mat. Sci. and Eng. 25 (1976) 3.

7. M. Cohen, "Metallurgy and the Evolution of Materials Science and Engineering," in Innovations in Ultrahigh-Strength Steel Technology, ed. G.B. Olson, M. Azrin, and E.S. Wright, Sagamore Army Materials Research Conference Proceedings: 34th (1987) p. 67.

8. G.B. Olson, "New Steels By Design," J. Materials Ed., in press.

9. G.B. Olson, in Innovations in Ultrahigh-Strength Steel Technology, ed. G.B. Olson, M. Azrin, and E.S. Wright, Sagamore Army Materials Research Conference Proceedings: 34th (1987) p. 3.

10. G.L. Krasko and G.B. Olson, in Innovations in Ultrahigh-Strength Steel Technology, ed. G.B. Olson, M. Azrin, and E.S. Wright, Sagamore Army Materials Research Conference Proceedings: 34th (1987) p.677.

11. G.R. Speich, in Innovations in Ultrahigh-Strength Steel Technology, ed. G.B. Olson, M. Azrin, and E.S. Wright, Sagamore Army Materials Research Conference Proceedings: 34th (1987) p. 89.

12. R. Wagner and R. Kampmann, in Innovations in Ultrahigh-Strength Steel Technology, ed. G.B. Olson, M. Azrin, and E.S. Wright, Sagamore Army Materials Research Conference Proceedings: 34th (1987) p. 209.

13. G. Ghosh and G.B. Olson, Northwestern University, research in progress.

14. R. Hemphill, Carpenter Steel alloy AerMet100, patent pending.

15. A. Needleman, in Innovations in Ultrahigh-Strength Steel Technology, ed. G.B. Olson, M. Azrin, and E.S. Wright, Sagamore Army Materials Research Conference Proceedings: 34th (1987) p. 331.

16. G.N. Haidemenopoulos, G.B. Olson, and M. Cohen, in Innovations in Ultrahigh-Strength Steel Technology, ed. G.B. Olson, M. Azrin, and E.S. Wright, Sagamore Army Materials Research Conference Proceedings: 34th (1987) p.549.

17. C.J. MacMahon, Jr., in Innovations in Ultrahigh-Strength Steel Technology, ed. G.B. Olson, M. Azrin, and E.S. Wright, Sagamore Army Materials Research Conference Proceedings: 34th (1987) p. 597.

18. P.M. Anderson, J.S. Wang, and J. R. Rice, in Innovations in Ultrahigh-Strength Steel Technology, ed. G.B. Olson, M. Azrin, and E.S. Wright, Sagamore Army Materials Research Conference Proceedings: 34th (1987) p. 619.

19. G.L. Krasko, C. Li, R. Wu, A.J. Freeman, and G.B. Olson, research in progress.

20. M.E. Eberhart and J. M. MacLaren in Innovations in Ultrahigh-Strength Steel Technology, ed. G.B. Olson, M. Azrin, and E.S. Wright, Sagamore Army Materials Research Conference Proceedings: 34th (1987) p. 693.

21. J.F. Watton, G.B. Olson, and M. Cohen, in Innovations in Ultrahigh-Strength Steel Technology, ed. G.B. Olson, M. Azrin, and E.S. Wright, Sagamore Army Materials Research Conference Proceedings: 34th (1987) p. 705.

22. A. Bilyk, T. Chen, N. Akaiwa, H. Eguchi, and G.B. Olson, Northwestern University 750-C95 Materials Design Class Project Report. June 1989.